Accretion-Driven Evolution of Black Holes: Eddington Ratios, Duty Cycles, and Active Galaxy Fractions

Francesco Shankar[1,2] ⋆ David H. Weinberg[3], and Jordi Miralda-Escudé[4,5]

[1] *GEPI, Observatoire de Paris, CNRS, Univ. Paris Diderot, 5 Place Jules Janssen, F-92195 Meudon, France*
[2] *Max-Planck-Institut für Astrophysik, Karl-Schwarzschild-Str. 1, D-85748 Garching, Germany*
[3] *Department of Astronomy, Ohio State University, McPherson Laboratory, 140 W. 18th Ave., Columbus, OH 43210-1173, USA*
[4] *Institució Catalana de Recerca i Estudis Avançats, Barcelona, Spain*
[5] *Institut de Ciències del Cosmos, Universitat de Barcelona, Barcelona Spain*

ABSTRACT

We develop semi-empirical models of the supermassive black hole and active galactic nucleus (AGN) populations, which incorporate the black hole growth implied by the observed AGN luminosity function assuming a radiative efficiency ϵ and a distribution of Eddington ratios λ. By generalizing these continuity-equation models to allow a distribution $P(\lambda|M_{BH}, z)$ we are able to draw on constraints from observationally estimated λ distributions and active galaxy fractions while accounting for the luminosity thresholds of observational samples. We consider models with a Gaussian distribution of $\log \lambda$ and Gaussians augmented with a power-law tail to low λ. Within our framework, reproducing the high observed AGN fractions at low redshift requires a characteristic Eddington ratio λ_c that declines at late times, and matching observed Eddington ratio distributions requires a $P(\lambda)$ that broadens at low redshift. To reproduce the observed increase of AGN fraction with black hole or galaxy mass, we also require a λ_c that decreases with increasing black hole mass, reducing the AGN luminosity associated with the most massive black holes. Finally, achieving a good match to the high mass end of the local black hole mass function requires an increased radiative efficiency at high black hole mass. We discuss the potential impact of black hole mergers or a λ-dependent bolometric correction, and we compute evolutionary predictions for black hole and galaxy specific accretion rates. Despite the flexibility of our framework, no one model provides a good fit to all the data we consider; it is particularly difficult to reconcile the relatively narrow λ distributions and low duty cycles estimated for luminous broad-line AGN with the broader λ distributions and higher duty cycles found in more widely selected AGN samples, which typically have lower luminosity thresholds.

Key words: cosmology: theory – galaxies: active – galaxies: evolution – quasars: general

1 INTRODUCTION

Supermassive black holes reside at the center of most, if not all, massive galaxies. The masses of black holes are tightly correlated with properties of their galactic hosts, especially the velocity dispersions and masses of their stellar bulges (e.g., Ferrarese & Merritt 2000; Gebhardt et al. 2000; Häring & Rix 2004). If black holes grow principally by radiatively efficient accretion, then the statistics of quasars and active galactic nuclei (AGN) can be used to track the growth of the black hole population. One common approach to modeling this growth uses the black hole "continuity equation"

(Cavaliere et al. 1971; Small & Blandford 1992). Simple versions of such models have two free parameters: the radiative efficiency ϵ, which relates mass accretion rate to luminosity, and the Eddington ratio $\lambda = L/L_{Edd}$, which relates luminosity to black hole mass. With the simplifying assumption that all active black holes have the same fixed values of ϵ and λ, and that each black hole has a duty cycle (i.e., a probability of being active at a given time) that depends on mass and redshift, $U(M_{BH}, z)$, one can use the observed AGN luminosity function to infer the average rate at which mass is being added to each mass range of the black hole population, thus evolving the black hole mass function forward in time. Model assumptions can be tested by comparing to observational estimates of the local ($z = 0$) black hole mass function

⋆ E-mail: francesco.shankar@obspm.fr,   Marie Curie Fellow

(e.g., Salucci et al. 1998; Marconi et al. 2004; Shankar et al. 2004; Shankar, Weinberg, & Miralda-Escudé 2009, hereafter SWM).

The models presented in SWM made use of this simplifying assumption of fixed values of ϵ and λ. Our key findings were *(i)* that models with $\epsilon \approx 0.07$ and $\lambda \approx 0.25$ yield a reasonable match to the local black hole mass function, though these specific inferred parameter values are sensitive to remaining uncertainties in the bolometric AGN luminosity function, and *(ii)* that reproducing the observed luminosity function with these models required "downsizing" evolution, with the duty cycle for high mass black holes declining more rapidly with time than the duty cycle for low mass black holes. Additional constraints on duty cycles (apart from their relation to the fraction of active galaxies) can be inferred from AGN and quasar clustering (Haiman & Hui 2001; Martini & Weinberg 2001), although these constraints depend on the assumed level of scatter between AGN luminosity and the mass of the host dark matter halo. Reproducing the strong observed clustering of $z = 4$ quasars (Shen et al. 2007) requires duty cycles close to one and minimal scatter between luminosity and halo mass (White, Martini, & Cohn 2008; Shankar et al. 2010b). However, reconciling the duty cycles predicted by SWM with the lower redshift clustering ($z \approx 1.5$) measured by Shen et al. (2009) requires significant scatter ($\Sigma \approx 0.5\,\mathrm{dex}$) between luminosity and halo mass to lower the predicted clustering amplitude (Shankar, Weinberg, & Shen 2010).

In this paper we consider more general continuity-equation models than those in SWM, incorporating a distribution of Eddington ratios $P(\lambda)$, as well as allowing for possible redshift evolution or black hole mass dependence of characteristic λ values or average radiative efficiency. The motivation for these more general models is to make contact with a broader range of observations that offer additional constraints on AGN and black hole evolution. Most obviously, many authors have now used black hole masses inferred from linewidth measurements or host galaxy properties to directly estimate Eddington ratios, finding evidence for broad $P(\lambda)$ distributions that change with redshift and black hole mass (see Section 3.3 below for observational references). Active galaxy fractions provide another set of important constraints on models. In single-λ models the duty cycle $U(M_{\mathrm{BH}}, z)$ — the fraction of black holes of mass M_{BH} at redshift z that are active at a given time — follows simply from the ratio of the observed luminosity function to the calculated black hole mass function (see SWM). With a broad $P(\lambda)$, the definition of duty cycle depends on the adopted threshold in luminosity or Eddington ratio, and because observational samples inevitably include these thresholds, the observed active galaxy fraction also tests models of $P(\lambda)$Other authors have recently implemented continuity equation models with broad Eddington ratio distributions (Merloni & Heinz 2008; Yu & Lu 2008; Cao 2010), but their studies are limited to a few specific models. Our implementation here draws on some of the techniques introduced by Cao (2010) and also on techniques and ideas from Steed & Weinberg (2003), who attempted a broad-ranging study of black hole evolution within a general continuity equation framework. The broad $P(\lambda)$ models described here also provide a more general framework for modeling quasar and AGN clustering, a topic we will examine in future work.

Phenomenological models of the black hole population like those in this paper complement models based on hydrodynamic simulations (e.g., di Matteo et al. 2005) or semi-analytic models that tie quasar activity to major mergers of galaxies or dark matter halos (e.g., Kauffmann & Haehnelt 2000; Wyithe & Loeb 2003; Hopkins et al. 2006). The numerical and semi-analytic approaches adopt a more complete physical scenario for the mechanisms that drive black hole accretion, and they tie AGN to the underlying galaxy population by construction. However, it can be difficult to interpret the significance of discrepancies with observations, or to know whether observational successes imply that the physical assumptions are correct. Phenomenological models are free to be driven by the data, within the constraints imposed by the adopted parameterization.

The next section describes our methods for computing black hole evolution and duty cycles, and it summarizes the SWM estimate of the bolometric luminosity function that is our basic observational input. All of our models reproduce this luminosity function by construction. In Section 3 we describe our three basic models for $P(\lambda)$ — a δ-function, a Gaussian in $\log\lambda$, and a Gaussian plus a power-law tail to low λ — then examine their impact on mass function evolution and conduct a first comparison to observed λ distributions. In Section 4 we turn our focus to active galaxy fractions and discuss how data might favour redshift evolution and possibly mass dependence of $P(\lambda)$. In Section 5 we revisit the comparison to observed λ distributions, the impact of black hole mergers at the rate predicted by hierarchical galaxy formation models, the relation between specific black hole growth and specific star formation rate, and the impact of adopting a λ-dependent bolometric correction. In Section 6 we discuss our results highlighting some internal tensions between data sets and key tensions between models and data. We conclude in Section 7. The appendices present some details of our calculational methods and of our estimates of observed active galaxy fractions. Throughout the paper we use cosmological parameters $\Omega_m = 0.30$, $\Omega_\Lambda = 0.70$, and $h \equiv H_0/100\,\mathrm{km\,s^{-1}\,Mpc^{-1}} = 0.7$, and we compute the linear matter power spectra running the Smith et al. (2003) code with $\Gamma = 0.19$, and $\sigma_8 = 0.8$.

2   FORMALISM

2.1   Evolving the black hole mass function

To study the global evolution of the black hole population through time, we develop models in which the black hole mass function is self-consistently evolved via the continuity equation,

$$\frac{\partial n_{\mathrm{BH}}}{\partial t}(M_{\mathrm{BH}}, t) = -\frac{\partial(\langle \dot{M}_{\mathrm{BH}} \rangle n_{\mathrm{BH}}(M_{\mathrm{BH}}, t))}{\partial M_{\mathrm{BH}}}, \qquad (1)$$

where $\langle \dot{M}_{\mathrm{BH}} \rangle$ is the mean accretion rate (averaged over the active and inactive populations) of the black holes of mass M_{BH} at time t (see, e.g., Cavaliere et al. 1971; Small & Blandford 1992; Yu & Tremaine 2002; Steed & Weinberg 2003; Marconi et al. 2004; Merloni 2004; Yu & Lu 2004; Tamura et al. 2006; SWM; Shankar 2009; Raimundo & Fabian 2009; Kisaka & Kojima 2010). This evolution is equivalent to the case in which every black hole grows constantly at the mean accretion rate $\langle \dot{M}_{\mathrm{BH}} \rangle$. In practice, indi-

vidual black holes turn on and off, but the mass function evolution depends only on the mean accretion rate as a function of mass. Note that Eq. (1) neglects any contribution from black hole mergers, which do not add mass to the black hole population but can alter the mass function by redistribution. In Section 5.3 we discuss the impact of including black hole mergers at the rate predicted by hierarchical models of structure formation.

We first define the Eddington ratio,

$$\lambda \equiv \frac{L}{L_{\mathrm{Edd}}}, \qquad (2)$$

where

$$L_{\mathrm{Edd}} \equiv l M_{\mathrm{BH}} = 1.26 \times 10^{38} \left(\frac{M_{\mathrm{BH}}}{\mathrm{M}_{\odot}} \right) \mathrm{erg\,s}^{-1} \qquad (3)$$

is the Eddington (1922) luminosity computed for Thomson scattering opacity and pure hydrogen composition. The growth rate of an active black hole of mass M_{BH} with Eddington ratio λ is $\dot{M}_{\mathrm{BH}} = M_{\mathrm{BH}}/t_{\mathrm{ef}}$, where the e-folding time is (Salpeter 1964)

$$t_{\mathrm{ef}} = 4 \times 10^8 \left(\frac{f}{\lambda} \right) \mathrm{yr} \equiv \frac{t_S}{\lambda}\,, \qquad (4)$$

with

$$f = \epsilon/(1-\epsilon) \quad \text{and} \quad \epsilon = \frac{L}{\dot{M}_{\mathrm{inflow}} c^2}. \qquad (5)$$

The radiative efficiency ϵ is conventionally defined with respect to the large scale mass inflow rate, but the black hole growth rate $\dot{M}_{\mathrm{BH}}$ is smaller by a factor of $(1-\epsilon)$ because of radiative losses.

We then define the probability for a black hole of a given mass M_{BH} to accrete at the Eddington ratio λ per unit $\log \lambda$, at redshift z as $P(\lambda|M_{\mathrm{BH}},z)$, normalized to unity, i.e., $\int d\log \lambda \, P(\lambda|M_{\mathrm{BH}},z) = 1$.[1] This is the quantity that can be related to the observed Eddington ratio distributions discussed in Section 1. The average growth rate of all black holes can be computed by convolving the input $P(\lambda|M_{\mathrm{BH}},z)$ with the duty cycle $U(M_{\mathrm{BH}},z)$

$$\langle \dot{M}_{\mathrm{BH}} \rangle = \int d\log \lambda \, P(\lambda|M_{\mathrm{BH}},z) \lambda \, U(M_{\mathrm{BH}},z) \frac{M_{\mathrm{BH}}}{t_{\mathrm{s}}}\,, \qquad (6)$$

where the integral extends over all allowed values of λ. A physically consistent model must have $U(\lambda, M_{\mathrm{BH}},z) \leqslant 1$ for all M_{BH} and z. In models where the Eddington ratio has a single value λ_1, $P(\lambda|M_{\mathrm{BH}},z) = \lambda_1 \delta(\lambda - \lambda_1)$, the duty cycle is simply the ratio of the luminosity and black hole mass functions,[2]

$$U(M_{\mathrm{BH}},z) = \frac{\Phi(L,z)}{\Phi_{\mathrm{BH}}(M_{\mathrm{BH}},z)}\,, \qquad L = \lambda l M_{\mathrm{BH}}\,. \quad (7)$$

This paper presents predictions from several models that take as input the observed luminosity function $\Phi(L,z)$, an assumed Eddington ratio distribution of active black holes, $P(\lambda|M_{\mathrm{BH}},z)$, and an assumed radiative efficiency ϵ, to solve Eq. (1) forwards in time. At each timestep, we use the black hole mass function $\Phi_{\mathrm{BH}}(M_{\mathrm{BH}},z)$ derived from the previous timestep (or from an assumed initial condition in the first timestep, and we compute the duty cycle $U(M_{\mathrm{BH}},z)$ by numerically solving the equation

$$\Phi(L,z) = \int d\log \lambda \, P(\lambda|M_{\mathrm{BH}},z) U(M_{\mathrm{BH}},z) \Phi(M_{\mathrm{BH}},z)\,, \quad (8)$$

$$M_{\mathrm{BH}} = L/(\lambda l)\,.$$

We then compute the average growth rate as a function of black hole mass via Eq. (6) and, finally, update the black hole masses and black hole mass function via the continuity equation (1).

Details of our numerical implementation are given in Appendix A. Directly solving Eq. 9 for $U(M_{\mathrm{BH}},z)$ is feasible for a discrete distribution of Eddington ratios. However, for all of the models discussed in this work, we will adopt *continuous* $P(\lambda|M_{\mathrm{BH}},z)$ distributions, which can be more efficiently handled following the method described by Steed & Weinberg (2003) and Cao (2010). The latter is based on solving Eq. 9 for the full mass function of *active* black holes

$$N_{\mathrm{act}}(M_{\mathrm{BH}},z) = \Phi_{\mathrm{BH}}(M_{\mathrm{BH}},z) \times U(M_{\mathrm{BH}},z)\,. \qquad (9)$$

More specifically, at any redshift z a parameterized active mass function $N_{\mathrm{act}}(M_{\mathrm{BH}},z)$ is derived by directly fitting[3] the AGN luminosity function $\Phi(L,z)$ at the same redshift via Eq. 9. The function $N_{\mathrm{act}}(M_{\mathrm{BH}},z)$ is then inserted in Eq. 1 by replacing $\langle \dot{M}_{\mathrm{BH}} \rangle n_{\mathrm{BH}}(M_{\mathrm{BH}},t) = \int d\log \lambda \, P(\lambda|M_{\mathrm{BH}},z) M_{\mathrm{BH}} N_{\mathrm{act}}(M_{\mathrm{BH}},z)/t_{\mathrm{s}}$, thus allowing the computation of the full black hole mass function $\Phi_{\mathrm{BH}}(M_{\mathrm{BH}},z)$ and the duty cycle $U(M_{\mathrm{BH}},z) = N_{\mathrm{act}}(M_{\mathrm{BH}},z)/\Phi_{\mathrm{BH}}(M_{\mathrm{BH}},z)$.

Eq. (1) is solved by imposing an initial condition that we fix, as in SWM, by assuming a constant value of the initial duty cycle. We usually choose this to be 0.5 at $z = 6$ for all masses, but in some models we lower it to 0.1 to allow the duty cycles at later times to be always lower than unity. The results at later redshifts are insensitive to the initial conditions for mass bins that have experienced substantial accretion growth (Marconi et al. 2004; SWM). Note that Eq. (1) could be solved backwards in time as well by forcing the initial condition to be the local black hole mass function (e.g., Merloni 2004). In this case, incorrect assumptions about the physical parameters or present day mass function manifest themselves as unphysical mass functions at earlier redshifts (e.g., negative space densities). Given the still substantial uncertainties in the local mass function (e.g., SWM; Vika et al. 2009; Shankar et al., in prep.) and our desire to explore a wide range of physical models, we prefer to evolve forward in time and compare to the local mass function as one of several observational constraints.

---

[1] Throughout the paper, log denotes base-10 logarithm and ln denotes natural logarithm.

[2] Following SWM, we will always use the symbol $\Phi(x)$ to denote mass and luminosity functions in logarithmic units of L or M_{BH}, i.e. $\Phi(x) d\log x = n(x) x \ln(10) dx$, where $n(x) dx$ is the comoving space density of black holes in the mass or luminosity range $x \to x + dx$, in units of Mpc^{-3} for $h = 0.7$. Unless otherwise stated, all masses are in units of $M_{\odot}$ and all luminosities are bolometric and in units of erg s^{-1}; e.g., $\log L > 45$ refers to quasars with bolometric luminosity $L > 10^{45}$erg s^{-1}.

[3] As discussed in Appendix A, we adopt a double power-law form for the input $N_{\mathrm{act}}(M_{\mathrm{BH}},z)$ which is a good (though not perfect) approximation of the functional form adopted for the AGN luminosity function (see Section 2.2). Our procedure allows us to reproduce the AGN luminosity function at the $\sim 5\%$ level, adequate precision given the statistical uncertainties in the data.
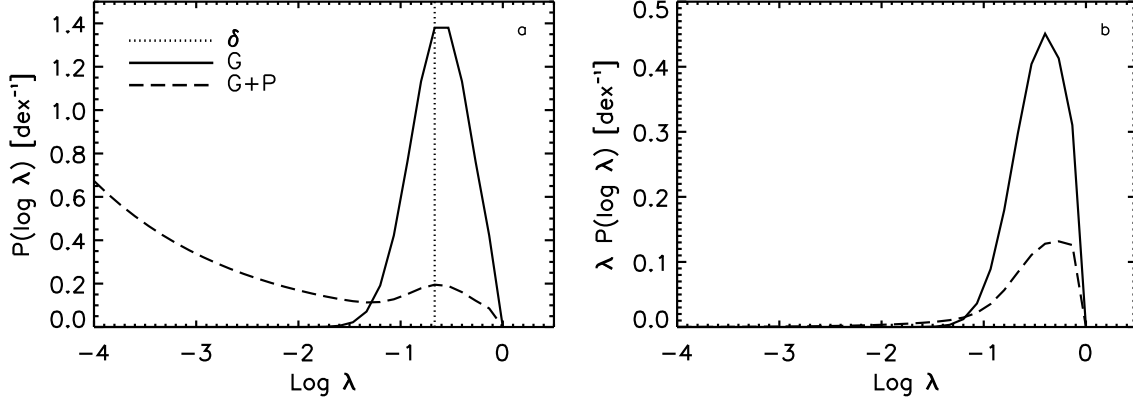
Figure 1. *Left*: Comparison among the three $P(\lambda)$ distributions taken as a reference throughout the paper. The *dotted* line is the δ-model centered on $\log \lambda_c = -0.6$, the *solid* line is the G-model, a Gaussian with dispersion of $\Sigma_\lambda = 0.3$ dex and centered around the same value of $\log \lambda_c = -0.6$, and the *long-dashed* line is the G+P-model, characterized by the same Gaussian plus a power-law with slope $\alpha = -0.3$ normalized to have the same value as the Gaussian at $\log \lambda = \log \lambda_c - \log \Sigma_\lambda$. Note that we define our distributions in $\log \lambda$ but refer to them in figures and text as $P(\lambda)$, and that all distributions are truncated at $\lambda = 1$. *Right*: Dimensionless emissivity per $\log \lambda$ interval, $\lambda P(\lambda)$, for the G and G+P distributions. Note that even the G+P model has its emissivity peak near the peak of the Gaussian component.

2.2 Input AGN Luminosity Function

A full discussion of our adopted AGN luminosity function appears in SWM; here we provide a brief summary [4]. A more detailed discussion can be found in SWM. We adopt the Ueda et al. (2003) fit to the number of sources per unit volume per dex of luminosity $\log L_X = \log L_{2-10\,\mathrm{keV}}$, composed of a double power-law and an evolution term:

$$\Phi(L_X, z) = e(z, L_X) \frac{A}{\left(\frac{L_X}{L^*}\right)^{\gamma_1} + \left(\frac{L_X}{L^*}\right)^{\gamma_2}},\qquad(10)$$

where

$$e(L_X, z) = \begin{cases} (1+z)^{p_1} & \text{if } z < z_c(L_X) \\ (1+z_c)^{p_1}[\frac{1+z}{1+z_c(L_X)}]^{p_2} & \text{if } z \geqslant z_c(L_X) \end{cases},\qquad(11)$$

with

$$z_c(L_X) = \begin{cases} z_c^* & \text{if } L_X \geqslant L_a \\ z_c^*(L_X/L_a)^{0.335} & \text{if } L_X < L_a \end{cases}.\qquad(12)$$

The values of the parameters have been tuned to correctly match the full set of data presented by SWM (see their Table 1).

The X-ray luminosity function of Eq. (10) is converted into a bolometric luminosity function using the fit to the bolometric correction given by Marconi et al. (2004), $\log L/L_X = 1.54 + 0.24\zeta + 0.012\zeta^2 - 0.0015\zeta^3$, with $\zeta = \log L/L_\odot - 12$, and $L_\odot = 4 \times 10^{33}$ erg s^{-1}. We have changed our procedure slightly with respect to SWM, dropping the convolution with 0.2-dex Gaussian scatter in bolometric correction, because the assumption that this scatter is uncorrelated with X-ray luminosity seems insecure. However, this change makes minimal difference to the derived luminosity function, and our results using the original SWM fit would not be noticeably different.

[4] The full tables of the input AGN luminosity functions, and also black hole mass functions and duty cycles (for a set of representative models), can be found in electronic format at http://mygepi.obspm.fr/~fshankar/.

The luminosity function data that we fit also include a number density of Compton-thick sources in each luminosity bin equal to the number of sources in the column density range $23 \leqslant \log N_H/\mathrm{cm}^{-2} \leqslant 24$, computed following the Ueda et al. (2003) prescriptions for the $P(N_H|L)$ column density distributions. We checked that our estimates of the Compton-thick number densities at high redshifts are fully consistent with the recent results by Alexander et al. (2011) and Fiore et al. (2011). As extensively discussed by SWM, the integrated intensity obtained from our model AGN luminosity function is also consistent with all the available data on the cosmic X-ray background for energies above 1 keV.

Our qualitative conclusions would not change if we adopted the Hopkins et al. (2007) luminosity function in place of SWM, though best-fit parameter values would be somewhat different.

3 EFFECTS OF A BROAD $P(\lambda)$

3.1 Input Eddington ratio distributions

In SWM we discussed accretion models for black holes with a single value of λ, examining the effects of redshift and mass dependence of this value of λ and describing the impact of uncertainties in the input AGN luminosity function related to its observational determination, obscured fractions, and bolometric corrections. From the match to the local black hole mass function, we were able to set constraints on the average input radiative efficiency and evolution in the characteristic λ. In this section we study the impact of broadening the input $P(\lambda)$ distribution. To this purpose we adopt and compare the outputs from three different distributions (shown in Figure 1):

- the δ-**model**, centered on $\log \lambda_c = -0.6$ (dot-dashed line in panel a; we choose this particular value because it provides a good match to the local black hole mass function);
- the **G-model**, a Gaussian in $\log \lambda$ with dispersion of
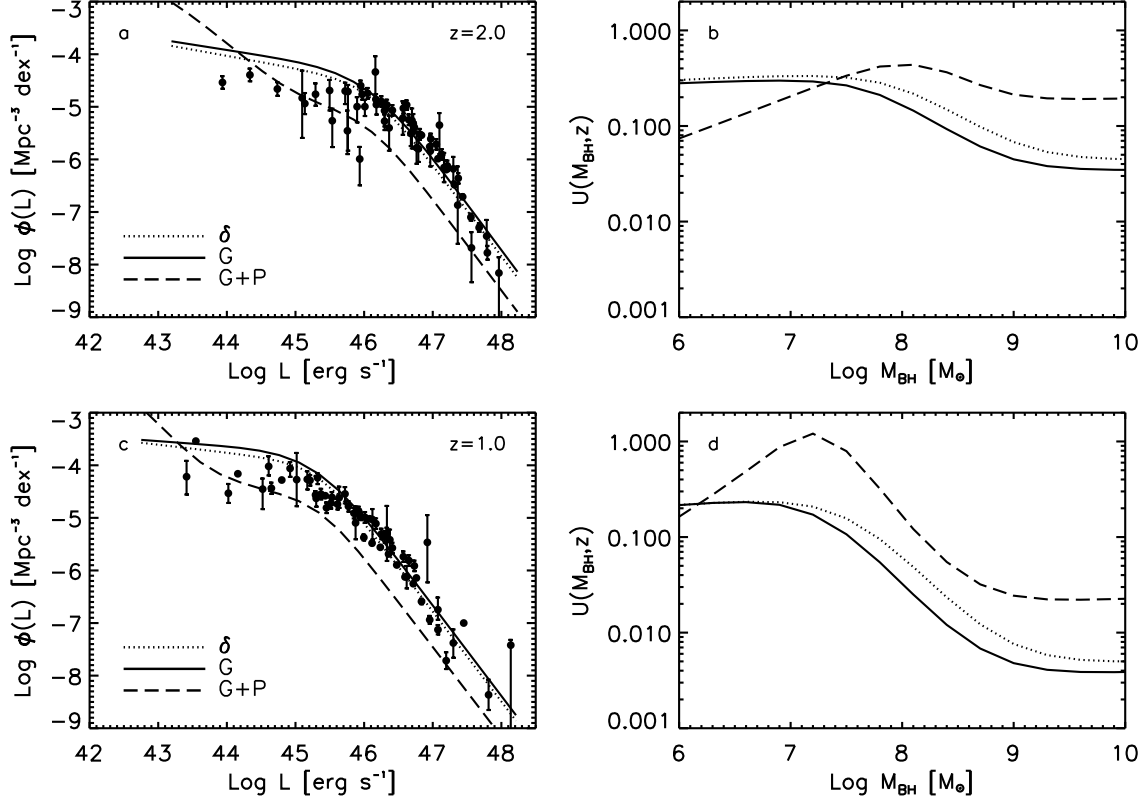
Figure 2. *Left panels*: Predicted luminosity function at $z = 2$ (top) and at $z = 1$ (bottom) for the three $P(\lambda)$ distributions of Figure 1, as labelled, when the *same* black hole mass function $\Phi_{\mathrm{BH}}(M_{\mathrm{BH}}, z)$ and duty cycle $U(M_{\mathrm{BH}}, z)$ are used, in this case the one predicted by the δ-model. Points show the data compilation of SWM. *Right panels*: predicted duty cycle $U(M_{\mathrm{BH}}, z)$ at the same redshifts $z = 2$ and $z = 1$ when, instead, the AGN luminosity function is *fixed* to the one in SWM, as in our self-consistent models. Allowing a large fraction of sub-Eddington accretion rates, as in the G+P model, increases the probability and thus the duty cycle for more massive black holes to be active at different luminosities.

$\Sigma_\lambda = 0.3$ dex and centered around the same value of $\log \lambda_c = -0.6$ (long-dashed line in panel a);

• the **G+P-model**, characterized by the same Gaussian plus a power-law with slope $\alpha = -0.3$ normalized to have the same value as the Gaussian at $\log \lambda = \log \lambda_c - \log \Sigma_\lambda$ (panel b).

For all models we adopt a radiative efficiency of $\epsilon = 0.06$, unless otherwise stated. The G+P distribution has a shape close to the one inferred by Kauffmann & Heckman (2009; see also Aird et al. 2011) in the local Universe from the Sloan Digital Sky Survey (SDSS), and it is also consistent with some theoretical and semi-empirical expectations (e.g., Merloni & Heinz 2008; Yu & Lu 2008; Hopkins & Hernquist 2009; Shen 2009). In particular, the power-law component could represent the effect of either a steady decline in the accretion rate after a near-Eddington growth phase or a second mode of AGN fueling triggered by secular instabilities instead of major mergers. In future sections and figures we will consider many variants on these three basic models, and we provide a full list of models in Table 1 for reference.

The left panels of Figure 2 illustrate the effect of varying the input Eddington ratio distribution $P(\lambda)$ at fixed duty cycle $U(M_{\mathrm{BH}}, z)$ and fixed black hole mass function $\Phi_{\mathrm{BH}}(M_{\mathrm{BH}}, z)$, at $z = 2$ and $z = 1$. The luminosity function in each case is computed via the convolution of the respective $P(\lambda)$ distributions with the product of the duty cycle

and black hole mass function (eq. 9). We *fix* $U(M_{\mathrm{BH}}, z)$ and $\Phi_{\mathrm{BH}}(M_{\mathrm{BH}}, z)$ to the one predicted by the δ-model (evolved in accord with the observed luminosity function), so that we can isolate the impact of varying the input $P(\lambda)$ distribution. Switching from a δ-function $P(\lambda)$ to a Gaussian of $\Sigma_\lambda = 0.3$ dex has a mild impact on the predicted luminosity function. However, adopting the G+P distribution at fixed $U(M_{\mathrm{BH}}, z)$ drastically lowers the luminosity function at high L, since the probability is dominated by low Eddington ratios. The shape of $\Phi(L, z)$ parallels that of the other models above the break luminosity, but the G+P model has a steeper faint-end slope reflecting the contribution of low-λ activity.

The procedure we follow in the rest of this paper is to compute $U(M_{\mathrm{BH}}, z)$ for a given input $P(\lambda)$ distribution in a way to reproduce the observed AGN luminosity function. The right panels of Figure 2 show, at the same redshifts $z = 2$ and $z = 1$, the duty cycles inferred by matching the SWM luminosity function when adopting the three $P(\lambda)$ distributions and the same underlying $\Phi_{\mathrm{BH}}(M_{\mathrm{BH}}, z)$, again that of the δ-model. The duty cycles $U(M_{\mathrm{BH}}, z)$ for the δ and G models are similar, but they are several times larger for the G+P model at high masses. As described in SWM, the duty cycles must decrease with mass in order to reproduce the "downsizing" effect in AGN evolution (the characteristic AGN luminosity increases with redshift). In the G+P
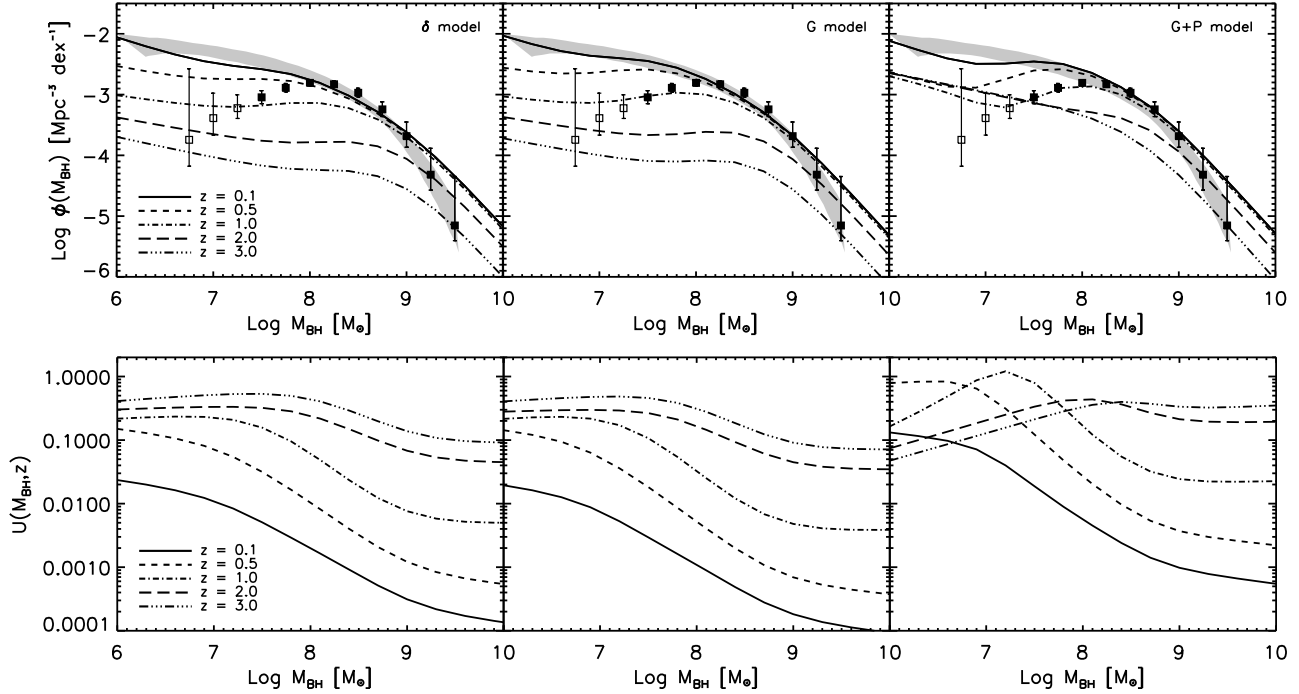
Figure 3. The *left*, *middle*, and *right* columns refer to outputs of the δ, G, and G+P models, respectively, whose $P(\lambda)$ distributions are shown in Figure 1. *Upper panels*: Predicted black hole mass function at $z \sim 0$ (*solid* lines) compared to the local estimates by SWM (*grey area*), and Vika et al. (2009; *squares* with error bars, with the *open* symbols indicating the estimates derived from galaxies below their reliability limit). Other lines show the predicted black hole mass function at earlier redshifts, as labelled. *Bottom panels*: Corresponding duty cycles (for all sources accreting above any $\lambda > 0$) as a function of black hole mass at different redshifts, as labelled. For all models a radiative efficiency of $\epsilon = 0.06$ has been assumed.

Model	shape & properties	Figures
δ	δ-function	$1-4$
G	Gaussian	$1-8$, 10
G+P	Gaussian+Power-Law	$1-8$
G(z)	Gaussian+$\lambda_c(z)$	7, 8, $10-12$, 16
G(z,$M_{\rm BH}$)	Gaussian+$\lambda_c(z, M_{\rm BH})$+low-z broadening+mass-dependent ϵ	$7-13$, 15, 16
G+P(z,$M_{\rm BH}$)	Gaussian+$\lambda_c(z, M_{\rm BH})$+z-dependent Power-Law+mass-dependent ϵ	7, 8, 11, 12
G(z,$M_{\rm BH}$)+constant ϵ	Gaussian+$\lambda_c(z, M_{\rm BH})$+low-z broadening	9
G(z,$M_{\rm BH}$)+K(λ)	G(z,$M_{\rm BH}$)+λ-dependent bolometric correction	15
G(z,$M_{\rm BH}$)+$\epsilon(z)$	Gaussian+$\lambda_c(z, M_{\rm BH})$+low-z broadening+z-dependent ϵ	9
G(z,$M_{\rm BH}$)+P($z < 0.7$)	G($z, M_{\rm BH}$) with steep power-law at $z < 0.7$	$7-9$, 12

Table 1. List of models explored in this work and figures in which they appear. The Gaussian always has dispersion of $\log \Sigma_\lambda = 0.3$ dex except for the models with broadening, for which $\log \Sigma_\lambda$ steadily increase with decreasing redshift as in Eq. (17). The redshift and mass dependence in the characteristic Eddington ratio λ_c are defined in Eqs. (15) and (16). If no evolution is assumed then $\log \lambda_c = -0.6$. The power-law component of the Eddington distribution is always normalized to have the same value as the Gaussian at $\log \lambda = \log \lambda_c - \log \Sigma_\lambda$, and a slope in $\log \lambda$ of $\alpha = -0.3$. In the last quoted model the power-law has slope $\alpha = -0.9$ and is normalized to have the same value as the Gaussian at $\log \lambda = \log \lambda_c - 0.2 \log \Sigma_\lambda$. The input radiative efficiency can be constant or vary with mass or redshift (see Eqs. 19 and 20) as detailed for each model.

model the duty cycle reaches unity at masses $\sim 10^7 M_\odot$, although with low values of λ for the majority of them. The decline of the duty cycle in this model at masses lower than $M_{\rm BH} \lesssim L_*/(l\lambda_c)$, where L_* is the break of the luminosity function (Eq. [10]), is induced by the presence of many AGNs radiating at low λ from high mass black holes, which can already account for the low-luminosity AGNs. However, the detailed form of this decline is sensitive to the precise shape of the AGN luminosity function and our assumed $P(\lambda)$.

3.2 Global Accretion Histories

Figure 3 shows the evolution of the black hole mass functions and duty cycles for the δ, G, and G+P models, respectively. In the upper panels, grey bands show the estimate of the local black hole mass function by SWM. The width of this band already encompasses a number of systematic uncertainties, but, as SWM discuss, the inferred mass function for $M_{\rm BH} < 10^8 M_\odot$ is sensitive to uncertainties in the treatment of spiral galaxy bulges. Vika et al. (2009) have tried to
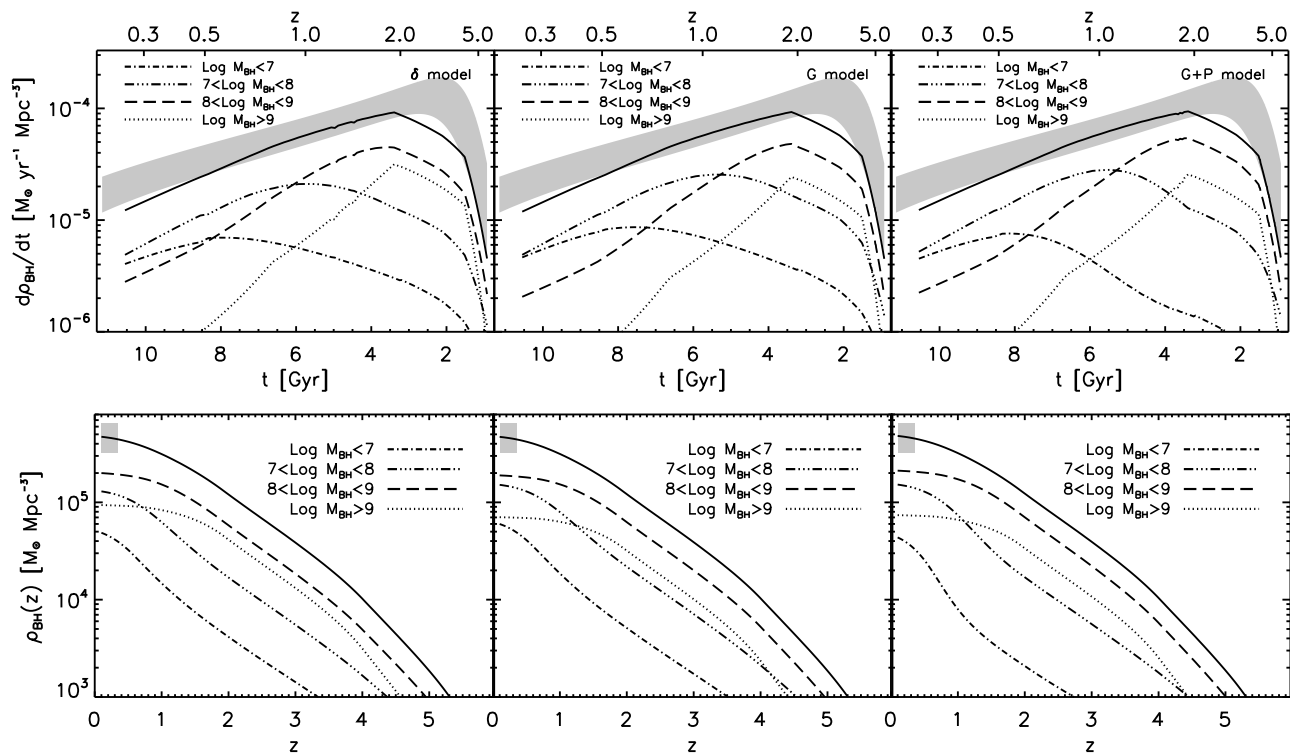
Figure 4. *Upper panels*: Growth rate of the integrated black hole mass density as a function of time (*solid* lines) and relative contributions of black holes of different final mass, as labelled; the *grey area* marks the 3σ uncertainty region of the cosmological star formation rate as inferred by Hopkins & Beacom (2006), scaled by a factor of 6.5×10^{-4}. *Lower panels*: predicted cumulative black hole mass density as a function of redshift (*solid* lines), and contributions of black holes of different mass, as labelled. The gray bar indicates local estimates of ρ_{BH}, which span a substantial range.

address this problem by estimating the local black hole mass function on an object by object basis, i.e., by computing the bulge fraction for each galaxy in a large sample, assigning black hole masses from an M_{BH}-L relation, and then computing the black hole mass function applying the $V/V_{\max}$ method. Their result, shown with open and filled squares in Figure 3, agrees well with SWM at high masses, while it turns over at $M < 10^8 M_{\odot}$ rather than continuing to rise to lower masses. We thus consider Vika et al.'s and SWM's results to broadly bracket the still remaining uncertainties in the determination of the local black hole mass function, and we will use both as a reference when comparing with models.

Moving from the δ-model to the G-model makes almost no difference to the evolution of the black hole mass function or to its $z = 0$ value. Both predictions are insensitive to our assumed initial conditions at $z = 6$ because even by $z = 4$ the accumulated mass from accretion greatly exceeds that in the initial seed population. The G+P model differs in this regard because reproducing the $z = 6$ luminosity function even with a duty cycle of 0.1 requires a high space density of seed black holes, since many black holes are active at low λ values that do not contribute to the observed range of the luminosity function. Once the evolved black hole mass function substantially exceeds the seed population, evolution is similar to that of the δ and G models. A high black hole space density at $z = 6$ is at odds with the strong quasar clustering observed at $z \approx 4$ by Shen et al. (2007), which requires duty cycles close to unity for black holes with $\lambda \gtrsim 0.1$

(White et al. 2008; Shankar et al. 2010b). We conclude that broad $P(\lambda)$ distributions at very high redshifts are observationally untenable, a conclusion in qualitative agreement with the findings of Cao (2010). If $P(\lambda)$ does have a long tail to low λ values, it must develop after the earliest stages of black hole growth; we will consider models with growing power-law tails in Section 4.

Duty cycles $U(M_{\mathrm{BH}}, z)$ tend to decline with redshift and with mass, for the reasons already explained in Figure 2. We note again the higher values of the duty cycle in the G+P model at all redshifts. The high-redshift curves are still affected by the initial conditions in the black hole population at low masses.

Figure 4 tracks the overall growth of the black hole population in bins of mass. In the upper panels, solid lines show the growth rate of the integrated black hole mass density $d\rho_{\mathrm{BH}}/dt(z)$ as a function of redshift, while the other lines show the mass density accreted in selected bins of *current* black hole mass, as labelled. As already noted by several groups (e.g., Marconi et al. 2004; Merloni et al. 2004; Merloni & Heinz 2008; SWM), the total $\rho_{\mathrm{BH}}(z)$ closely matches the shape of the cosmological star formation rate (SFR), here taken from Hopkins & Beacom (2006; with the gray area marking their 3-σ contours) and re-scaled by an *ad hoc* factor of 6.5×10^{-4}, close to the ratio between black hole mass and stellar mass measured in the local Universe (e.g., Häring & Rix 2004). All three models again show a clear signature of downsizing in their accretion histories. The accretion onto the very massive black holes with log $M_{\mathrm{BH}}/M_{\odot} > 8$ always
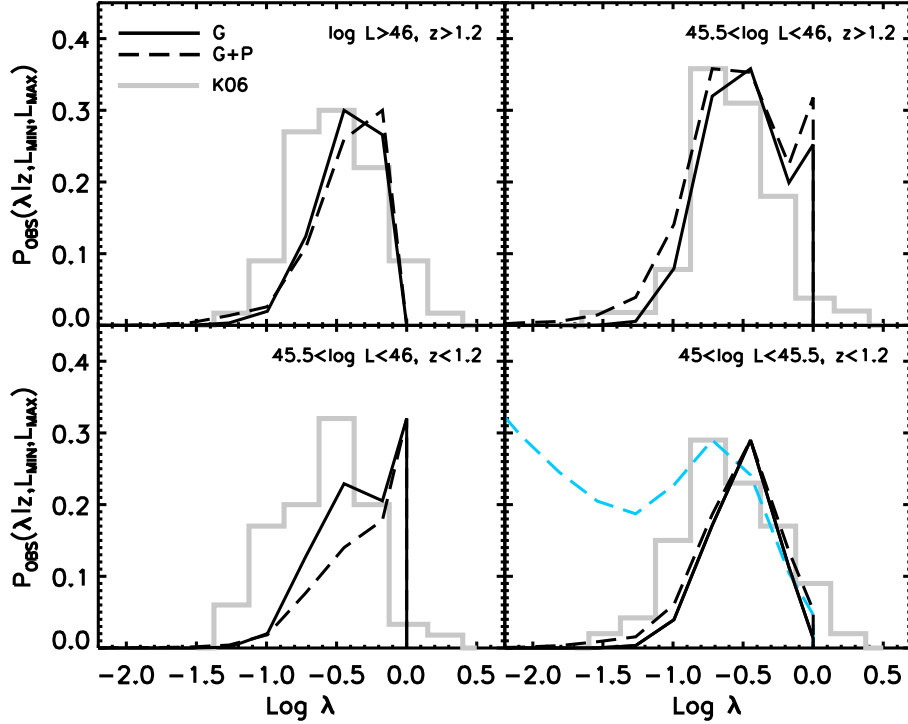
Figure 5. Eddington ratio distributions predicted by the G (*solid* lines) and G+P (*long-dashed* lines) models, compared to the K06 data (*grey histograms*) for black holes in the range $10^7 < M_{\rm BH}/M_\odot < 10^{10}$ at different redshift and luminosity bins, as labelled. The predictions have been estimated at the average redshifts of $z = 1$ and $z = 2$ for the low and high-z subsamples, respectively, although the predictions do not strongly depend on these choices if no redshift dependence in the $P(\lambda)$ is included. The *cyan long-dashed line* in the lower-right panel is the G+P model prediction when no lower luminosity threshold is considered.

peaks at $z \sim 2$, concurrent with the peak in the emissivity of luminous optical quasars (e.g., Osmer 1982; Richards et al. 2006; Croom et al. 2009). The less massive black holes with $7 < \log M_{\rm BH}/M_\odot < 8$ are characterized by a much broader peak centered at $z \sim 1-1.5$. The lower panels show the cumulative mass density of all black holes with mass $10^6 < M_{\rm BH}/M_\odot < 10^{10}$ (solid lines), and the mass density accreted onto black holes of different current mass, as labelled. By construction, all models share the same radiative efficiency and therefore accumulate the same total mass densities at any time. They differ only slightly with respect to the total mass accumulated in different mass bins. The solid grey square indicates the total mass density in black holes at $z = 0.1$ derived from the local black hole mass function.

Figures 3 and 4 show that the evolution of the black hole mass function is insensitive to the shape of $P(\lambda)$, provided the characteristic value λ_c and the input AGN luminosity function are held fixed. This reassuring result indicates that earlier studies assuming a single λ value (e.g., Marconi et al. 2004; Shankar et al. 2004; SWM) reached robust results for mass function evolution. This is essentially because in our G+P model, with power-law slope $\alpha = -0.3$, the emissivity per logarithmic interval of λ is dominated by the Gaussian peak (Figure 1b). A steeper slope would yield duty cycles greater than unity and is therefore not allowed. Even our G+P model is disfavored at high redshifts because the observed quasar clustering implies that the most massive black holes should be active at large values of λ with high duty cycles. Our model results are obviously dependent on the value of λ_c, which changes the location of the break in the

black hole mass function, and the value of ϵ, which affects the normalization (see SWM and Section 4 below).

3.3   Comparison with measured $P(\lambda)$ distributions

Drawing on virial mass estimators grounded in reverberation mapping studies (e.g., Wandel, Peterson, & Malkan 1999; Vestergaard 2002; McLure & Jarvis 2004) and the availability of large samples of quasar spectra from wide field surveys, several groups have inferred the distribution of Eddington ratios in different ranges of redshift and luminosity. Kollmeier et al. (2006; hereafter K06) measured $P(\lambda)$ from the AGN and Galaxy Evolution Survey (AGES; Kochanek et al. 2011), finding that luminous AGNs at $0.5 < z < 3.5$ have a quite narrow range of Eddington ratios, with a peak at $\lambda \sim 0.25$ and a dispersion (including observational errors) of ~ 0.3 dex. Netzer et al. (2007), analyzing quasar samples from the SDSS, found a similar result, with a slightly larger dispersion, from a sample centred at $z \sim 2.5$. Netzer & Trakhtenbrot (2007, see also Vestergaard 2004; McLure & Dunlop 2004), analyzing nearly ten thousand SDSS quasars in the redshift range $0.3 \lesssim z \lesssim 0.75$, confirmed the log-normal shape of the Eddington ratio distribution and also found evidence for a significant decrease with time in the characteristic λ_c defining the peak of the distribution. K06 also found a factor ~ 3 decrease in the peak value of λ between high and low redshifts for the more massive black holes in their sample. Many other studies of the Eddington ratio distributions of quasars and active galaxies have found evidence for time evolution of λ_c, and in some cases
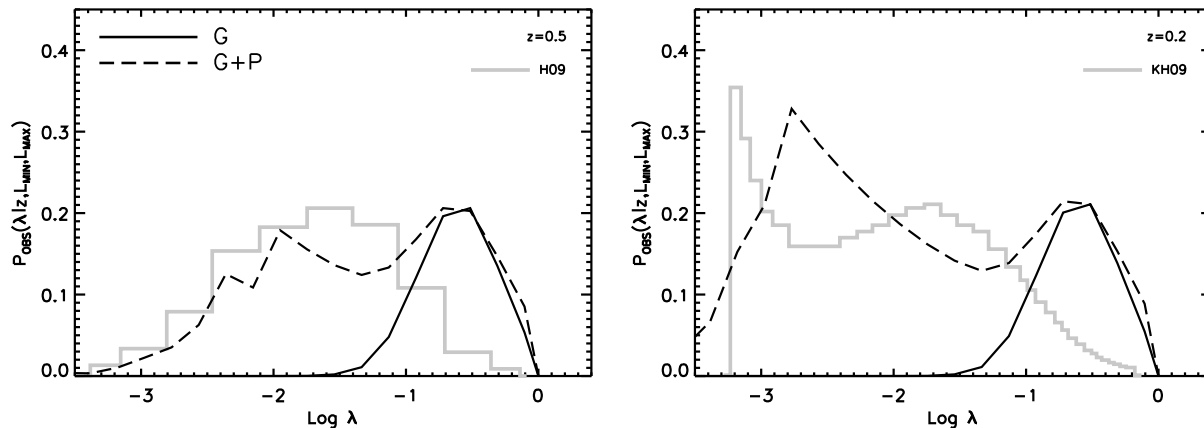
Figure 6. Eddington ratio $P(\lambda)$ distributions predicted by the G (*solid* lines) and G+P (*long-dashed* lines) models at lower redshifts. *Left panel*: Predictions compared to the H09 data (*grey histogram*) for black holes in the range $10^7 < M_{\rm BH}/M_\odot < 10^{10}$ with $\log L > 43.5$ at $z = 0.5$. *Right panel*: Predictions compared to the KH09 data (*grey histogram*) for black holes in the range $10^7 < M_{\rm BH}/M_\odot < 10^8$ with $\log L > 42.5$ at $z = 0.2$.

for mass-dependence (e.g., McLure & Dunlop 2004; Vestergaard 2004; Heckman et al. 2005; Ballo et al. 2007; Babić et al. 2007; Bundy et al. 2008; Rovilos & Georgantopoulos 2007; Cao & Li 2008; Fine et al. 2008; Shen et al. 2008; Greene et al. 2009; Hickox et al. 2009; Kauffmann & Heckman 2009; Kelly et al. 2010; Shankar et al. 2010e; Steinhardt & Elvis 2010a,b; Trakhtenbrot et al. 2011; Willott et al. 2010a,b; Aird et al. 2011; Shen & Kelly 2011). However, sample selection, observational noise, and intrinsic scatter in black hole mass estimators can all have strong effects on the apparent distribution of Eddington ratios (e.g., Lamastra et al. 2006; Lauer et al. 2007; Marconi et al. 2008; Shen et al. 2008; Netzer 2009; Shen & Kelly 2010; Rafiee & Hall 2011). At low redshifts, where samples can probe to much lower AGN luminosities, it is clear that the distribution of Eddington ratios is much broader than the roughly log-normal distribution found for optically luminous quasars at high redshift.

As a set of representative examples of the literature, we consider the Kollmeier et al. (2006; K06 hereafter) results for broad-line optically luminous quasars at $z > 0.5$, the Hickox et al. (2009; H09 hereafter) results at $z \approx 0.5$ for a sample selected by X-ray, infrared, and radio emission, and Kauffmann & Heckman's (2009; KH09 hereafter) analysis of the local AGN population in the SDSS, with an effective redshift $z \approx 0.2$.

To make a close comparison of our models to observed samples of AGNs, we compute Eddington ratio distributions conditioned to active AGNs with luminosities between $L_{\rm min}$ and $L_{\rm max}$, $P_{\rm obs}$, as

$$P_{\rm obs}(\lambda|z, L_{\rm min}, L_{\rm max}) = \quad (13)$$
$$A \sum_k \sum_j P(\lambda = L_k/(M_{\rm BH,j} l)|z, M_{\rm BH,j}) N_{\rm act}(M_{\rm BH,j}, z)$$

where $N_{\rm act}(M_{\rm BH}, z)$ is defined in Eq. 9. The sums in the above equation are extended to all bins of black hole mass, and to all bins of luminosity in the assumed observed range, $L_{\rm min} < L_k < L_{\rm max}$. Since we are interested here in the *shapes* of the predicted Eddington distributions, the constants A are chosen to renormalize the $P_{\rm obs}(\lambda|z, L_{\rm min}, L_{\rm max})$ to match the peaks of the observed distributions.

Figure 5 compares the Eddington ratio distributions predicted by the G and G+P models to the K06 data, for black holes in the range $10^7 < M_{\rm BH}/M_\odot < 10^{10}$ in four different bins of redshift and luminosity. The predictions have been computed at the redshifts of $z = 1$ and $z = 2$ for comparison to the $z < 1.2$ and $z > 1.2$ subsamples, respectively. The predictions do not strongly depend on these choices, since $P(\lambda)$ has no explicit redshift dependence. Both models predict, essentially by construction, a roughly log-normal $P(\lambda)$ with a typical λ_c that agrees with the K06 measurements. Most importantly, the power-law tail of the G+P model does *not* lead to substantial disagreement because the fraction of quasars of a fixed luminosity with low values of λ is much less than the fraction of black holes of a fixed mass with the same low values of λ. In fact, the λ distribution for all quasars with any luminosity (cyan dashed curve in the lower right panel) has the same shape as our assumed intrinsic distribution in Figure 1a. The most significant disagreement with the data is the high characteristic λ for $45.5 < \log L < 46$ at $z < 1.2$ (lower left panel), a consequence of keeping the model λ_c fixed instead of allowing redshift evolution.

Figure 6 compares the predicted and observed λ distributions for the lower redshift samples of H09 at $z \approx 0.5$ and KH09 at $z \approx 0.2$. To roughly take into account the effective limits in black hole mass and luminosity of the observational samples, for the former we consider all black holes with $M_{\rm BH} > 10^7 M_\odot$ shining at $L > 10^{43}\,{\rm erg\,s^{-1}}$, while in the latter case we adopt the restricted range $10^7 < M_{\rm BH}/M_\odot < 10^8$ shining above $L = 10^{42.5}\,{\rm erg\,s^{-1}}$. The match to the observations is poor in both cases. The distributions predicted by the G model are much narrower than the observed distributions, and they peak at a value $\lambda_c \approx 0.25$ that is roughly ten times higher than the high-λ peaks of the observed distributions. The power-law tail in the G+P model is in rough agreement with the observed distributions at low λ, but the peak of the Gaussian component remains discrepant. Fitting these observations, even approximately, requires evolution of λ_c, decreasing towards low redshift. We return to this point in Section 5.2 below, after first finding independent evidence for evolution in λ_c from observed active galaxy fractions.
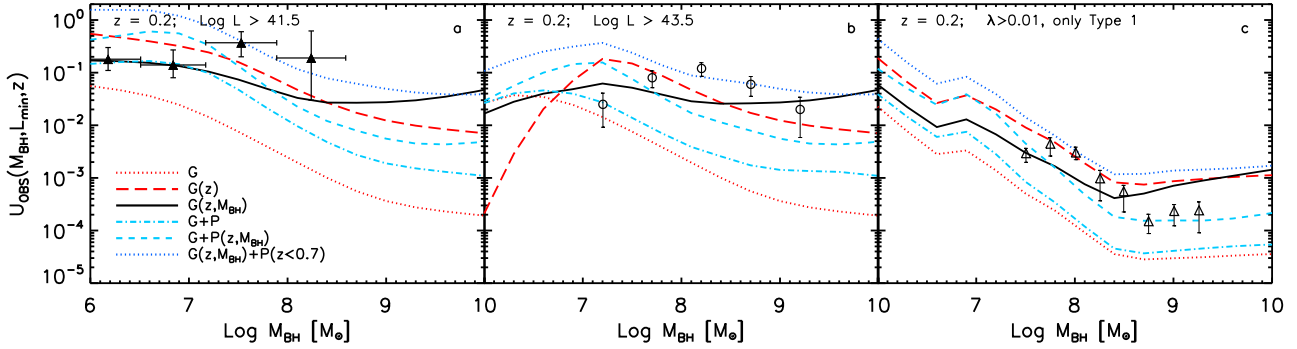
Figure 7. Comparison of predicted and observationally estimated duty cycles at low redshift. *Left panel*: Data points from Goulding et al. (2010) compared to model predictions at $z = 0.2$ as labelled, with a luminosity threshold $\log L > 41.5$. *Middle panel*: Data points from Kauffmann et al. (2003) compared to model predictions, with a luminosity threshold $\log L > 43.5$. *Right panel*: Data points from Schulze & Wisotzki (2009) compared to model predictions, with an *Eddington ratio* (not luminosity) threshold $\lambda > 0.01$ and a correction factor for the Type 1 Broad Line AGNs taken from Greene & Ho (2009). The three lowest mass points include the Schulze & Wisotzki (2010) incompleteness corrections, which are negligible at higher mass.

4   ACTIVE GALAXY FRACTIONS: REDSHIFT AND MASS-DEPENDENCE OF $P(\lambda)$

Duty cycles are a basic prediction of continuity equation models as discussed in Section 2. If we assume that most or all massive galaxies contain black holes, as supported by observations of the local universe (see, e.g., Ferrarese & Ford 2005, and references therein), then active galaxy fractions can be used as an observable proxy for black hole duty cycles. However, active galaxy fractions depend on the luminosity or Eddington ratio threshold of each specific observational sample: lower thresholds obviously increase the active fraction. Therefore, in order to properly compare model predictions to available data sets, we define the fraction of black holes shining above a luminosity threshold $L_{\min}$, or observed duty cycle U_{obs}, as

$$U_{\mathrm{obs}}(M_{\mathrm{BH}}, L_{\min}, z) = \int_{\log \lambda_{\min}}^{\infty} P(\lambda | M_{\mathrm{BH}}, z) U(M_{\mathrm{BH}}, z) d\log\lambda , \quad (14)$$

$$\lambda_{\min} = L_{\min}/(l M_{\mathrm{BH}}) .$$

There are several systematic uncertainties involved in predicting this observed duty cycle, including the determination of the effective $L_{\min}$ or $\lambda_{\min}$, incompleteness of the AGN catalogs, and the observational estimates of black hole masses and their abundances. Nonetheless, even the qualitative trends with redshift and black hole mass are enough to provide strong model tests.
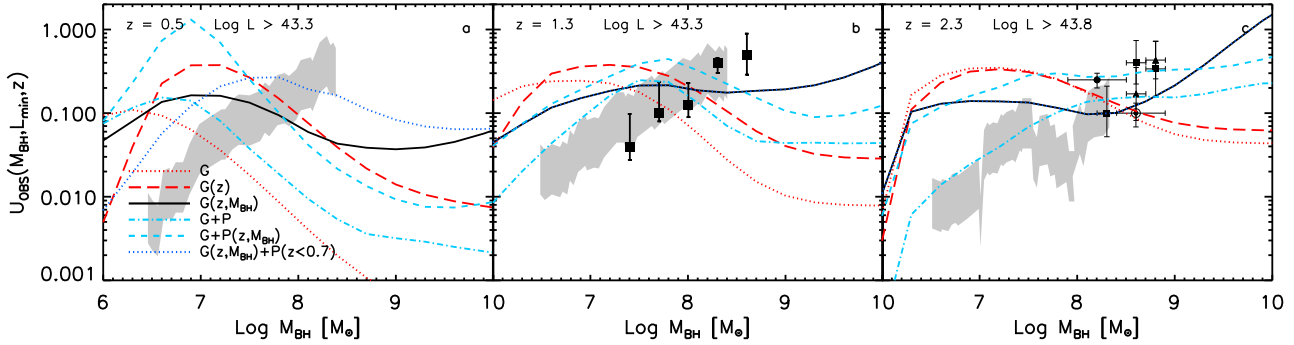
4.1   Observational Estimates

We first summarize the observational estimates of AGN fractions that we adopt for our model comparisons, with further details of some of these estimates given in Appendix D. For high luminosity, broad-line (Type 1) AGN in the local Universe, Schulze & Wisotzki (2010) have estimated the mass function of active black holes at $z < 0.3$ by applying linewidth mass estimators to quasars identified in the Hamburg/ESO objective prism survey. They divide their active black hole density by the total black hole space density in the Marconi et al. (2004) mass function to derive an active fraction. Schulze & Wisotzki impose a threshold of $\lambda \geqslant 0.01$ in their estimated Eddington ratio to de-

fine active systems. Host galaxy contamination causes incompleteness in their AGN catalog below $M_{\mathrm{BH}} \approx 10^{7.5} M_{\odot}$ (for $\lambda \geqslant 0.01$). In the right panel of Figure 7 we plot the points from their Figure 12, correcting their three lowest M_{BH} points for incompleteness as suggested by the authors. According to their simulations, higher M_{BH} points should be unaffected by incompleteness, and we have omitted points below $M_{\mathrm{BH}} = 10^7 M_{\odot}$ where incompleteness corrections become large. The active black hole fractions estimated by Schulze & Wisotzki (2010) are low, only $\sim 2 \times 10^{-4}$ at $M_{\mathrm{BH}} = 10^9 M_{\odot}$, rising to $\sim 10^{-3}$ at $M_{\mathrm{BH}} = 10^8 M_{\odot}$.

Kauffmann et al. (2003) estimate much higher active fractions for narrow line (Type 2) AGN identified by applying emission line diagnostics to SDSS spectra in the SDSS main galaxy redshift survey. Since Kauffmann et al. (2003) begin with a galaxy catalog, quasars that are bright enough to appear as point sources (rather than extended sources) in SDSS imaging are excluded. They estimate their completeness limit at $10^7 L_{\odot}$ in [OIII] luminosity, which we convert to an approximate $L_{\min} = 10^{43.5} \mathrm{erg\,s^{-1}}$ by adopting an extinction-corrected bolometric correction of ~ 800 (both Kauffmann et al. 2003 and KH09 adopt extinction-corrected luminosities). Points in the middle panel of Figure 7 are taken from Figure 5 of Kauffmann et al. (2003), where we have simply converted stellar mass to black hole mass by multiplying by 1.6×10^{-3} (Magorrian et al. 1998). This crude conversion should be reasonably accurate above $M_* \sim 10^{11.5} M_{\odot}$, but it probably overestimates the black hole mass for lower mass galaxies that are no longer bulge-dominated. The Kauffmann et al. (2003) active fractions rise from $\sim 2\%$ at $M_{\mathrm{BH}} = 10^9 M_{\odot}$ to $\sim 10\%$ at $M_{\mathrm{BH}} = 10^8 M_{\odot}$, then decline towards lower M_{BH}. The $10^{43.5} \mathrm{erg\,s^{-1}}$ luminosity threshold corresponds to $\lambda = 0.01$ at $M_{\mathrm{BH}} \approx 10^{7.5} M_{\odot}$, so at higher masses the Kauffmann et al. (2003) estimates correspond to a lower λ-threshold than Schulze & Wisotzki's.

The 1.5 to 2 order-of-magnitude gap between the Kauffmann et al. (2003) and Schulze & Wisotzki (2009) active fractions can be partly explained by the different abundances of broad line and narrow line AGN at low redshift. The abundance ratio of the two types of AGN has been addressed by Greene & Ho (2009; a correction of Greene & Ho 2007), who analyze all SDSS spectroscopic objects (tar-

Figure 8. Predicted and observationally estimated duty cycles at redshifts $z = 0.5$, $z = 1.3$, and $z = 2.3$. In all panels, *grey bands* show the estimates of Xue et al. (2010). Points in the *middle* panel, points are from Bundy et al. (2008). Points in the *right* panel come from Erb et al. (2006; *filled small squares*), Kriek et al. (2007; *filled triangles*), Alexander et al. (2005; 2008; *filled circle*), and Caputi et al. (2006; *semi-filled circle*).

geted as galaxies or quasars) in Data Release 4 (Adelman-McCarthy et al. 2006) to define a sample of 8,400 broad-line AGN at $z \lesssim 0.3$. Their estimated active fractions (in their Figure 11) are close to those of Schulze & Wisotzki. They find a gap of 0.9-1.3 dex between their active black hole mass function for broad-line AGN and the corresponding result (Heckman et al. 2004) for SDSS narrow-line AGN (see Greene & Ho 2009, Figure 10), which implies a correction of $\sim 10 - 20$ for the ratio of Type I to Type II AGN at low redshift. The remaining factor of $5 - 10$ may be accounted for by the effects of scatter in bolometric corrections, different luminosity thresholds, and systematic offsets in the black hole mass function estimates. Note that scatter in $L_{bol}/L_{[OIII]}$ could make the effective luminosity threshold of the Kauffmann et al. (2003) data lower than we have assumed, in particular if the luminosity function is affected by a steeply rising low-λ tail in $P(\lambda)$.

For studies that probe to lower AGN luminosities, active galaxy fractions are even higher than those of Kauffmann et al. (2003). For example, Ho (2004) argues that at least 40% of local bulge-dominated galaxies host a low luminosity AGN and/or a LINER, and Grier et al. (2011) find nuclear X-ray sources in $\sim 60\%$ of galaxies in the SINGS survey (Kennicutt et al. 2003). As a representative example of low luminosity statistical studies, we show in the left panel of Figure 7 the data of Goulding et al. (2010, their Figure 5), based on an X-ray and IR census of a volume-limited sample of galaxies with $D < 15$ Mpc. Their active fractions range from 14% to 37% over the black hole mass range $10^6 - 10^{8.5} M_\odot$, albeit with large statistical errors reflecting the small sample size. The luminosity threshold of this sample is very low and about $L_{min} = 10^{41.5}$ erg s^{-1} in bolometric units (their Figure 3).

At higher redshifts we take as our primary data set the measurements reported by Xue et al. (2010) based on moderate luminosity X-ray AGN in the Chandra Deep Fields. We reproduce results from their Figure 14 (the upper, or-ange bands) as grey bands in the three panels of Figure 8, converting their X-ray luminosity thresholds to bolometric luminosity thresholds with our luminosity-dependent bolometric correction (Section 2.2). We again convert stellar masses to black hole masses by simply multiplying by the Magorrian et al. (1998) factor of 1.6×10^{-3}. This scaling should be taken with a grain of salt, as we are using total

stellar masses rather than bulge masses and ignoring possible redshift evolution of the scaling factor. However, these uncertainties should not affect the key lessons that we take from Xue et al. (2010): at all three redshifts, the duty cycle for BHs shining above $\log L > 43.3$, increases with increasing M_{BH} (indicated in the data by increasing M_*), and for the most massive galaxies active fractions are $10-50\%$ (grey bands marking the 1-σ uncertainty).

Other points in Figure 8 come from other studies with similar redshift ranges and luminosity thresholds. At intermediate redshifts, the data of Bundy et al. (2008) from the DEEP2 and AEGIS surveys show nearly the same mass trend and normalization as Xue et al. (2010). More recently, Mainieri et al. (2011) also found evidence for a steep increase in AGN activity with stellar mass at $\langle z \rangle \approx 1.1$, though with a luminosity threshold about two orders of magnitude higher than the one by Xue et al. (2010). At $z > 2$ we add several points for high mass black holes based on the studies of Caputi et al. (2006), Erb et al. (2006), Kriek et al. (2007), and Alexander et al. (2005, 2008). These data have been collected at bolometric luminosities approximately $\log L > 43.8$, comparable to those of Xue et al. (2010). Further details about these observations are discussed in Appendix D. They extend the mass trend found by Xue et al. (2010), with active fractions ranging from $\sim 10\%$ to $\sim 50\%$.

4.2 Low-redshift AGN fractions: A redshift-dependent $P(\lambda)$?

Red dotted and cyan dot-dashed curves in Figure 7 show the duty cycles $U(M_{BH}, z)$ predicted by the G and G+P models at $z = 0.2$, where we have imposed the bolometric luminosity thresholds $\log L > 41.5$ (left panel), $\log L > 43.5$ (middle), and $\lambda > 0.01$ (right). For the right panel, we have additionally multiplied model predictions by a mass-dependent factor (ranging from $\sim 15\%$ at $M_{BH} = 10^7 M_\odot$ to $\sim 3\%$ at $M_{BH} = 3 \times 10^8 M_\odot$) to account for Greene & Ho's (2009) estimate of broad line AGN fractions. (Specifically, the correction is obtained from the ratio of Broad Line to Type II number densities in their Figure 10, with an extrapolation of their results above $M_{BH} \sim 5 \times 10^8 M_\odot$.) Both models drastically underpredict all measured active fractions for $M_{BH} > 10^{7.5} M_\odot$. Predicted duty cycles are higher for the

G+P model, and the gap between G+P and G is larger for lower luminosity thresholds that allow a larger contribution of sub-Eddington black holes, but the G+P model still falls well short of the observed active fractions.

As introduced by Shankar et al. (2004) and discussed more extensively by SWM (see their Figure 11), one can increase predicted duty cycles at low redshift by adopting a redshift-dependent Eddington ratio distribution, with characteristic λ_c that drops towards low redshifts. Decreasing $\lambda_c \propto L/M_{\rm BH}$ maps a given luminosity to more massive, and hence rarer, black holes, thus requiring a higher duty cycle to reproduce the observed AGN space density. Furthermore, the results of H09, KH09, and other studies directly suggest a lower λ_c at low redshifts, as already discussed in Section 3.3 (see Figure 6). Motivated by these results, we introduce models in which the location of the peak in the G and G+P $P(\lambda)$ distributions decreases from $\lambda_c = 1.0$ at $z = 6$ to $\lambda_c \sim 0.02$ at $z \sim 0.1$, following

$$\lambda_c(z) = \lambda(z = 6) \left[\frac{1+z}{7} \right]^{\alpha} , \qquad (15)$$

with $\alpha = 2.2$, although we note that even lower values of α yield similar results. Eq. 15 implies $\lambda_c = 0.71, 0.48, 0.29, 0.16, 0.06, 0.03, 0.02$ at $z = 5, 4, 3, 2, 1, 0.5$, and 0.1, respectively.

In agreement with SWM, who considered δ-function $P(\lambda)$, we find that this evolution has a minor impact on the evolved black hole mass function (at least at high masses) or on the global accretion histories shown in Figure 4. However, predicted duty cycles at $z \sim 0.2$ for the G(z) model — a Gaussian $P(\lambda)$ with the $\lambda_c(z)$ given by Eq. 15 — are much higher than those of the G model, as shown by comparing the dotted and long-dashed curves in Figure 7. The model now approximately agrees with the Goulding et al. (2010), Kauffmann et al. (2003), and Schulze & Wisotzki (2010) active fractions, though at high masses it is above the latter data and below the former two. Solid and short-dashed curves in Figure 7 show models with Gaussian and G+P λ-distributions that incorporate both redshift and mass dependence of λ_c, as discussed in the next section.

The redshift dependence expressed in Eq. 15 is by no means unique. In particular, we have checked that an equally good match to the local data can be obtained by allowing the characteristic λ_c to decrease only below redshift $z \sim 1$, while remaining close to unity at higher redshifts. This abrupt change in λ_c at late times leads to duty cycles that increase at fixed black hole mass from $z \sim 1$ to $z \sim 0$, instead of decreasing as predicted by continuous redshift evolution. This increasing behaviour may be in conflict with observations; some direct X-ray and optical analyses show that the fraction of active galaxies above a fixed stellar mass decreases with decreasing redshift in the range $0 < z < 1$ (e.g. Shi et al. 2008).

4.3   AGN fractions vs. mass: A mass-dependent $P(\lambda)$?

Figure 8 compares the model predictions to the higher redshift active fraction data discussed in Section 4.1. The G and G(z) models both predict a duty cycle that declines with increasing $M_{\rm BH}$, opposite to the trend found by Xue et al. (2010) and Bundy et al. (2008). At first glance, the

G+P model appears to fare better, at least in the $z = 1.3$ and $z = 2.3$ panels. However, we view this better agreement as artificial — it is a consequence of the high initial black hole space density required to keep high-z duty cycles below unity in this model (see Figure 3). The high black hole space density inherited from these initial conditions leads to a lower duty cycle for low mass black holes. We regard these high initial space densities as observationally untenable for the reasons discussed in Section 3.2, so we discount this apparent success of the G+P model, which vanishes by $z = 0.5$ in any case.

The only other way we have found to make the predicted duty cycle increase with black hole mass at these redshifts is to introduce an explicit mass dependence of $P(\lambda)$, with λ_c declining with increasing mass. In this case massive black holes are matched to more common, lower luminosity AGN, implying a higher duty cycle. There is some direct empirical support for such a trend (e.g. Heckman et al. 2004; Ballo et al. 2007; Babić et al. 2007; Netzer & Trakhtenbrot 2007; Rovilos & Georgantopoulos 2007; Fine et al. 2008; H09), and it could arise theoretically in models that envisage a faster shut-off of activity in more massive systems due to AGN feedback (e.g., Matteucci 1994; Granato et al. 2006; Lapi et al. 2006). Motivated roughly by these empirical studies, we have adopted a model with the same redshift dependence as before and a mass dependence

$$\log \lambda_c(M_{\rm BH}, z) = \log \lambda_c(z) + [\beta_M (\log M_{\rm BH} - C)] , \quad (16)$$

with $\beta_M = -0.3$ and $C = 7$. Eq. 16 implies a λ_c that drops by a factor of two between $10^7 M_\odot$ and $10^8 M_\odot$ and by a further factor of two between $10^8 M_\odot$ and $10^9 M_\odot$.

Solid lines in Figures 7 and 8 show predictions of the G($z, M_{\rm BH}$) model, which incorporates mass-dependence of the radiative efficiency ϵ as well as of λ_c, for reasons that we will discuss shortly. This model also incorporates a broadening of the Gaussian in the G($z, M_{\rm BH}$) at lower redshifts following the trend

$$\log \Sigma_\lambda(z) = \log \Sigma_\lambda(z = 6) - 0.4 \log \left(\frac{1+z}{7} \right) , \qquad (17)$$

with $\log \Sigma_\lambda(z = 6) = 0.3$, yielding $\Sigma_\lambda(z) \sim 0.4, 0.5, 0.6$ at $z = 3, 2, 0.2$. As discussed below, we include this additional modification to the model to provide a better match to the local Eddington ratio distributions. At all redshifts, this model predicts a duty cycle that is roughly flat or rising with black hole mass, though the rising trend is always weaker than that found by Xue et al. (2010) and Bundy et al. (2008). We could adopt a still stronger mass dependence in this model, which would improve agreement with the observed trends, but this would no longer be supported by empirical estimates (e.g., Hickox et al. 2009), and it would exacerbate problems in explaining the Eddington ratio distributions and local black hole mass function (see below). The G($z, M_{\rm BH}$) model is also in rough agreement with all the local data sets on active fractions (solid lines in Figure 7), though it overpredicts the Schulze & Wisotzki (2010) active fractions for $M_{\rm BH} \sim 10^9 M_\odot$ by a factor of several.

Short-dashed lines in Figure 8 show the predictions of a model labeled G+P($z, M_{\rm BH}$) that has a G+P form with redshift- and mass-dependent λ_c and mass-dependent ϵ like that of the G($z, M_{\rm BH}$) model. Instead of allowing the Gaussian to broaden at low redshift via Eq. 17, we keep its width
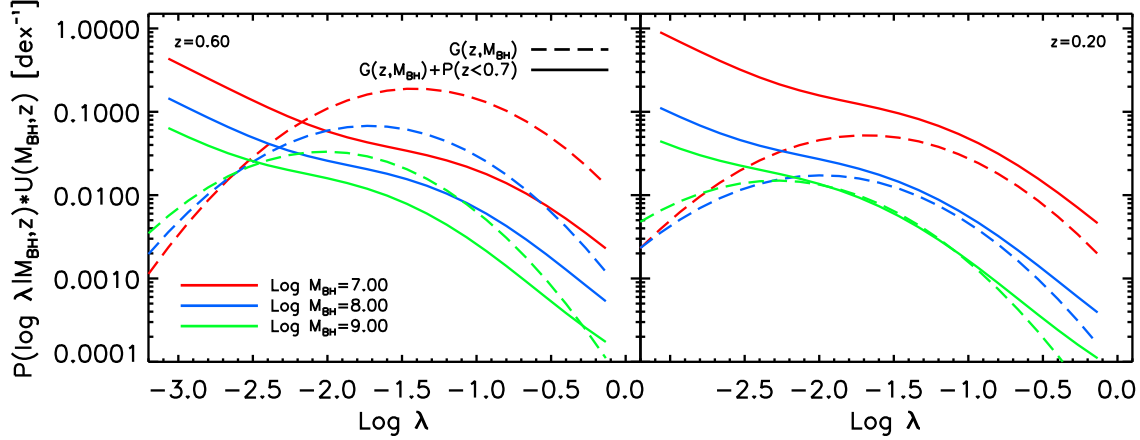
Figure 9. $P(\lambda)$ distributions for our $G(z, M_{BH})$ model (*dashed* curves) and the $G(z, M_{BH})$ model with a steep power-law component added at low redshift (*solid* curves), shown at $z = 0.6$ (*left*) and $z = 0.2$ (*right*). In each panel, the three curves show $P(\lambda)$ for black hole masses of $10^7 M_\odot$, $10^8 M_\odot$, and $10^9 M_\odot$, as labelled.

fixed at $\Sigma_\lambda = 0.3$ but allow the power-law tail to grow over time. Specifically, the $P(\lambda)$ distribution is cut off at

$$\lambda_{\min}(z) = 0.1 \left(\frac{1+z}{7}\right)^3 , \qquad (18)$$

implying $\lambda_{\min} = 0.1$, 0.063, 0.036, 0.019, 0.0079, 0.0023, 0.0098, 0.00039 at $z = 6$, 5, 4, 3, 2, 1, 0.5, 0.1. This simple modification (similar to that adopted by Cao 2010) avoids the need for a large initial black hole seed population, thus removing the artificial aspect of our redshift-independent G+P model, but it produces a full G+P distribution at intermediate and low redshifts. The predictions of this model are similar to those of $G(z, M_{BH})$, with a somewhat worse match to the $z = 1.3$ data in Figure 8b and a somewhat better match to the Schulze & Wisotzki data in Figure 7. Both models fail to reproduce the rising $U(M_{BH})$ found at $z = 0.5$ by Xue et al. (2010).

4.4 AGN fractions vs. mass: a steep power-law component at low z?

At early stages of our investigation, we anticipated that the observed trends of rising active fraction with rising galaxy mass might be explained mainly by the combination of a broad $P(\lambda)$ with sample luminosity thresholds: high mass black holes remain observable at lower λ values, so they could have higher duty cycles above fixed luminosity even if the trend of total duty cycle (over all λ values) was flat or decreasing. This is essentially the explanation advanced by Aird et al. (2011), who fit AGN data from the PRIMUS survey with a model in which all black holes have an Eddington ratio distribution $P(\lambda) = P_0(z) \times (\lambda/\lambda_0)^{-0.7}$ independent of mass.

As already discussed in the context of our G+P model, we find that a long power-law tail is unrealistic at high redshift because it implies duty cycles higher than unity unless the population of seed black holes is implausibly large. However, a power-law component that kicks in at lower redshifts is still feasible. The blue dotted lines in Figures 7 and 8 show the predicted duty cycles for a model equivalent to $G(z, M_{BH})$ with the addition of a power-law component at

$z < 0.7$ with slope $\alpha = -0.9$ and normalized to have the same value as the Gaussian at $\log \lambda = \log \lambda_c - 0.2 \log \Sigma_\lambda$. Figure 9 plots $P(\lambda)$ for this model at three different black hole masses and two redshifts, in comparison to those of the $G(z, M_{BH})$ model. For this plot we have multiplied $P(\lambda)$ by $U(M_{BH}, z)$ so that the curves are normalized to the duty cycle rather than integrating to unit probability. The Gaussian and power-law components join to produce a $P(\lambda)$ that is close to a single power law from $\lambda = 10^{-3}$ to $\lambda = 1$.

This model still exhibits "downsizing" in the sense that higher mass black holes have lower duty cycle at any given λ. However, the duty cycle for AGN active above a luminosity threshold $\log L = 43$ *increases* with black hole mass, as shown in the left panel of Figure 8, because massive black holes can shine above the threshold at low λ. This is the only model we have constructed that reproduces the Xue et al. (2010) trend at $z = 0.5$. The Aird et al. (2011) prescription, with the $P(\lambda)$ normalization independent of mass, would produce a still stronger rising trend, but we find that such a model cannot simultaneously match our evolved black hole mass function and our input luminosity function.

5 OTHER OBSERVATIONAL CONSTRAINTS

5.1 The local mass function: A mass-dependent radiative efficiency?

As shown previously in Figure 3, our simple, non-evolving δ, G, and G+P models yield reasonable agreement with SWM's estimate of the local black hole mass function for $M_{BH} \leqslant 10^9 M_\odot$, but the model predictions skirt the upper boundary of the observational estimates at higher masses. Figure 10 plots mass functions for the Gaussian $P(\lambda)$ models with various assumptions about redshift evolution and mass-dependence. Redshift evolution alone (red long-dashed line) produces modest changes above $\sim 2 \times 10^8 M_\odot$, but the decreasing λ_c boosts growth of high mass black holes at the expense of low mass black holes, leading to a flattening of $\Phi(M_{BH})$ near $10^8 M_\odot$ and a lower space density of lower mass black holes. This change partly reproduces the
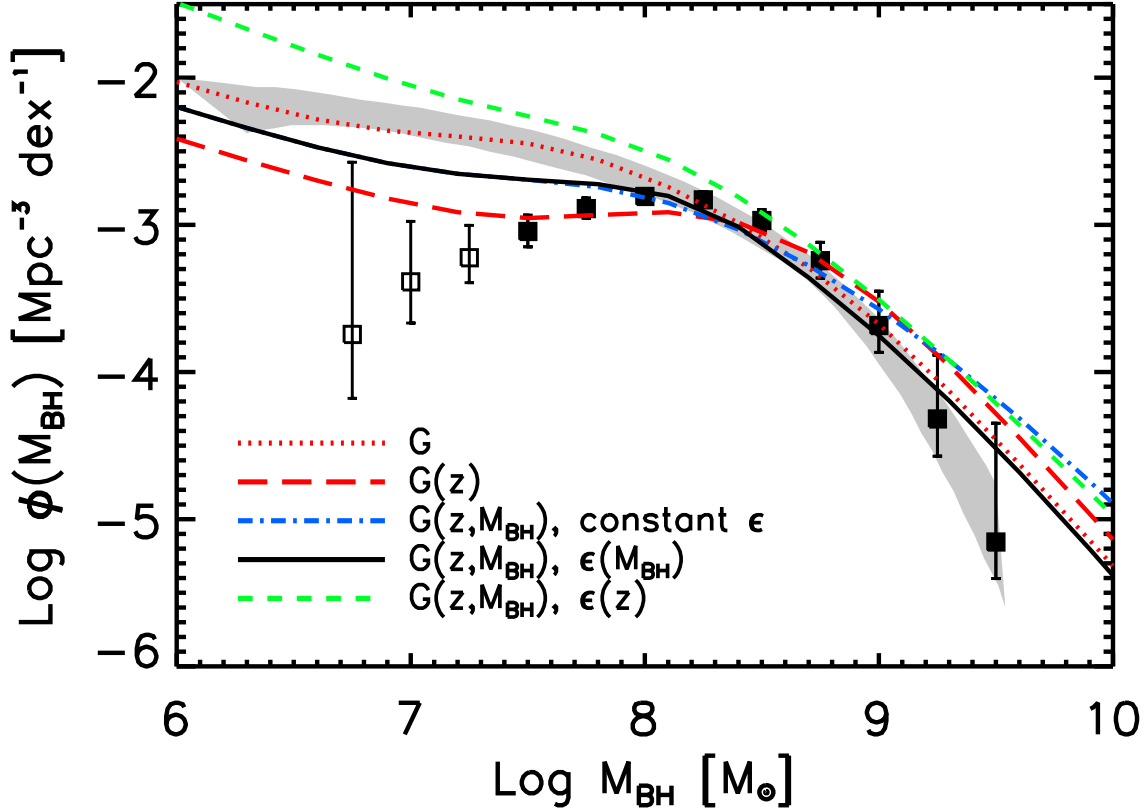
Figure 10. Local black hole mass function predicted by different models, as labelled. Data are as in Figure 3. Of the three G(z, M_{BH}) models, with mass-dependent λ_c, only the one with mass-dependent ϵ (solid line) matches the high end of the mass function. Elsewhere in the paper this preferred model is simply labeled G(z, M_{BH}).

turnover found by Vika et al. (2009), though it still does not reproduce their estimate below $M_{\mathrm{BH}} \sim 10^{7.5} M_\odot$.

Adding only the mass-dependent λ_c of Eq. 16 leads to the "G(z, M_{BH}), constant ϵ" curve (blue dot-dashed line) in Figure 10. For this model, we have lowered the radiative efficiency from $\epsilon = 0.06$ to $\epsilon = 0.05$ to improve the match to the amplitude of $\Phi(M_{\mathrm{BH}})$ at $10^8 - 10^{8.5} M_\odot$, where it is best measured. However, the model then strongly overpredicts the mass function at $M_{\mathrm{BH}} > 10^9 M_\odot$, a direct consequence of the higher duty cycles of high mass black holes that the model was designed to produce. As discussed in Section 5.3 below, the expected impact of black hole mergers would make this overprediction even more severe.

Volonteri, Sikora & Lasota (2007), Cao & Li (2008), and Fanidakis et al. (2011), among others, have suggested that radiative efficiency may increase with black hole mass, perhaps mirroring a merger-induced increase in the average spin for the more massive black holes. Cao & Li (2008) claimed evidence for an increasing ϵ from the match between the predicted and local black hole mass functions at the high-mass end. More recently Davis & Laor (2011) directly determined the radiative efficiency from the ratio between bolometric luminosity and accretion rate, the latter determined from thin accretion disk model fits to the optical luminosity density. Their analysis seems to support an increase of the radiative efficiency with black hole mass, from 0.03 at low masses to 0.4 at high masses. An increasing radiative efficiency at high masses is also consistent with the notion that the bulk of luminous radio AGNs, believed to be rapidly spinning black

holes, are indeed massive black holes (e.g., McLure & Jarvis 2004; Metcalf & Magliocchetti 2006; Shankar et al. 2008a,b; Shankar et al. 2010e).

Inspired by these theoretical and empirical arguments, we have constructed the G(z, M_{BH}) model (see Table 1), which, following Cao & Li (2008), adopts a mass-dependent ϵ given by:

$$\epsilon = \begin{cases} 0.05 & \text{if } M_{\mathrm{BH}} < 10^8 M_\odot \\ 0.05(M_{\mathrm{BH}}/10^8\,M_\odot)^{0.3} & \text{if } M_{\mathrm{BH}} \geqslant 10^8 M_\odot \end{cases}, \quad (19)$$

This change reduces the implied accretion rates of massive black holes, leading to much better agreement with the local $\Phi(M_{\mathrm{BH}})$ as shown by the solid curve in Figure 10. This model also has a stronger positive trend of duty cycle with M_{BH}, improving agreement with the data in Figure 8. The two improvements are connected: raising ϵ decreases the space density of massive black holes, so a higher duty cycle is required to match the space density of active black holes. The mass function (not shown) of the model introduced in Section 4.4, with a steep power-law at $z < 0.7$, is nearly identical to that of G(z, M_{BH}), except at $\log M \leqslant 7.2$, where it is lower by ~ 0.3 dex.

Wang et al. (2009) have instead recently claimed empirical evidence for an increase of ϵ with redshift. Their results are based on an inversion of Soltan's (1982) argument, expressing the radiative efficiency at any redshift as the ratio of the accreted mass density up to that redshift $\rho_{\mathrm{BH}}(z)$ to the corresponding total emissivity obtained by direct integration of the AGN luminosity function (see their

Eq. 6). The mass density $\rho_{\rm BH}(z)$ was computed by first measuring the mass density locked up in all active black holes at z (with masses from virial relations), then correcting by the duty cycle extracted from the number counts of active galaxies in VIMOS-VLT Deep Surveys. Clustering analysis also provides hints of redshift-dependent radiative efficiency. Shankar et al. (2010b), adopting basic accretion models and cumulative number matching arguments, found that black hole accretion plus merger models consistent with both the quasar luminosity function and the strong observed clustering at $z \approx 4$ (Shen et al. 2007) must be characterized by high duty cycles and large radiative efficiencies $\epsilon \gtrsim 0.2$, if they are accreting at a significant fraction of the Eddington limit. However, an efficiency $\epsilon \geqslant 0.2$ at all redshifts would underpredict the local black hole mass function (SWM). In flux-limited quasar surveys, higher redshift quasars are found above higher luminosity thresholds, so both of these empirical arguments could potentially be answered by a mass-dependence of the sort implied by Eq. 16.

We nonetheless consider a directly redshift-dependent model, approximating these empirical findings with the relation

$$\epsilon(z) = 0.0022 \left[1 + \mathrm{erfc}\left(-\frac{z}{1.5}\right)^6 \right]. \qquad (20)$$

Eq. (20) implies $\epsilon \approx 0.14, 0.14, 0.12, 0.05, 0.02, 0.01$ at $z = 6, 4, 2, 1, 0.5, 0.2$, respectively. The local black hole mass function predicted by this $\mathrm{G}(z, M_{\rm BH}) + \epsilon(z)$ model, shown by a green dashed curve in Figure 10, tends to overestimate the observed mass function at all scales. The match could be improved by increasing the overall normalization of $\epsilon(z)$, still allowed (and actually preferred) by the measurements of Wang et al. (2009; see their Figure 2a), but such an increase produces unphysical models with duty cycles significantly higher than unity, and it still leaves too many high mass black holes. Moreover, the cosmological accretion rate predicted by the $\mathrm{G}(z, M_{\rm BH}) + \epsilon(z)$ model is morphologically different from the cosmological star formation rate of galaxies, at variance with the agreement shown in Figure 4. In itself this is not a fatal objection, but it then requires non-trivial fine tuning to reproduce a tight local relation between black hole mass and stellar mass.

5.2 Eddington Ratio Distributions, Revisited

In any model with a broad $P(\lambda)$, the observable distribution of Eddington ratios depends on the luminosity of the AGN being considered. Figure 11 shows the contribution to the bolometric luminosity function from different ranges of λ at $z = 3.2$ (top panels) and $z = 0.3$ (bottom panels) in the $\mathrm{G}(z)$, $\mathrm{G}(z, M_{\rm BH})$, and $\mathrm{G+P}(z, M_{\rm BH})$ models (left, middle, and right panels, respectively). There is a natural trend for the high end of the luminosity function ($\log L > 46$) to be mainly contributed by high-λ black holes, with a broader range of λ contributing at lower luminosities. Interestingly, we find that the $\lambda < 0.01$ range does not dominate at any luminosity at any redshift. Only in the $\mathrm{G}(z, M_{\rm BH})$ model and at low redshifts are there roughly equal contributions to the luminosity function from each logarithmic bin of λ in the range $0.01 - 1.0$. This is important to compare with models that rely on a significant contribution from "ADAF-type" modes to the global accretion history of black holes

(see, e.g., Merloni & Heinz 2008 and Draper & Ballantyne 2010).

Figure 12 compares the Eddington ratio distributions of the $\mathrm{G}(z, M_{\rm BH})$, $\mathrm{G}(z)$, and $\mathrm{G+P}(z, M_{\rm BH})$ models (black solid, red long-dashed, and cyan dashed lines, respectively) to the observational estimates of K06, H09, and KH09, discussed earlier in Section 3.3. Beginning at low redshift (bottom panels), we see that the declining $\lambda_c(z)$ in the redshift-dependent models resolves the discrepancy seen in Figure 6, producing much better agreement with the H09 and KH09 data. The additional broadening in the Gaussian component (Eq. 17) produces excellent agreement with the H09 distribution and excellent agreement with KH09 for $\lambda > 10^{-2.5}$. The $\mathrm{G+P}(z, M_{\rm BH})$ model achieves similar agreement, matching KH09 slightly better at low luminosities but still falling short at $\lambda < 10^{-3}$. The blue dotted curves in the lower panels show the $\mathrm{G}(z, M_{\rm BH})$ model with the steep power-law at low z, introduced in Section 4.4. The predicted Eddington ratio agrees poorly with both the H09 and KH09 data.

At $z > 1.2$ (upper panels) model predictions are in approximate agreement the K06 data, with $\mathrm{G}(z)$ showing the best agreement. However, the $z = 1$ model outputs tend to disagree with the K06, $z < 1.2$ histograms (middle panels). We note that Netzer & Trakhtenbrot (2007) find a peak at $\lambda \approx 0.1$ for $M = 10^8 - 10^{8.5} M_\odot$ black holes at $z = 0.7$. Kelly et al. (2010) have also recently claimed an Eddington ratio distribution from SDSS of Broad Line Quasars that peaks at $L/L_{\rm Edd} \sim 0.05$ with a dispersion of ~ 0.4 dex. Both these results would be closer to the model predictions.

While the duty cycle data considered in Section 4.3 seem to favor a λ_c that decreases at higher $M_{\rm BH}$, the K06 data disfavor this solution. We note that the luminosity threshold of the Xue et al. (2010) study that motivates this model is much lower than that of the Kollmeier et al. data, $L_{\rm min} \sim 10^{43} \mathrm{erg\,s^{-1}}$ rather than $L_{\rm min} \sim 10^{45} - 10^{46} \mathrm{erg\,s^{-1}}$. A reconciliation of these results could therefore lie in a model that behaves differently in these two luminosity regimes.

5.3 The Impact Of Mergers

It is usually assumed that mergers of galaxies are followed by mergers of their central black holes, making black hole mergers a potentially important source of evolution in the black hole mass function (e.g., Hughes & Blandford 2003; Wyithe & Loeb 2003; Islam et al. 2004; Scannapieco & Oh 2004; Yoo & Miralda-Escudé 2004; Volonteri et al. 2005; Lapi et al. 2006; Yoo et al. 2007; Marulli et al. 2008; Bonoli et al. 2009; Shen 2009; SWM; Bonoli et al. 2010; Shankar 2010; Shankar et al. 2010a,d; Shankar et al. 2011; Kocsis & Sesana 2011; Kulkarni & Loeb 2011). We will save a full discussion of mergers for future work, but here we briefly assess their potential impact on the mass function. Improving on our simplified calculation in SWM, we here follow the schemes proposed by Shen (2009) and Shankar et al. (2010b), computing the rate of black hole mergers from the halo merger rate predicted from fits to N-body dark matter simulations (Fakhouri & Ma 2008), corrected by a dynamical friction timescale. In the presence of mergers the continuity equa-
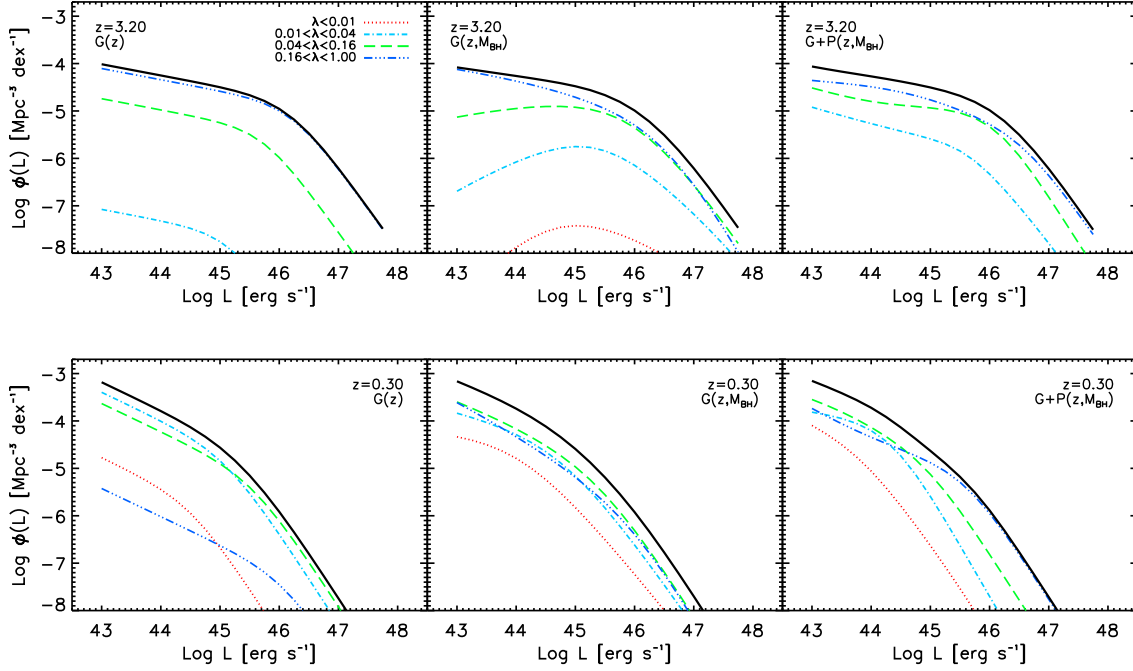
Figure 11. Contributions of different Eddington ratio distributions to the overall bolometric luminosity functions at $z = 3.2$ (top) and $z = 0.3$ (bottom), as predicted by the G(z), G($z, M_{\rm BH}$), and G+P($z, M_{\rm BH}$) models (left, middle, right panels, respectively).

tion reads as

$$\frac{\partial n_{\rm BH}}{\partial t}(M_{\rm BH}, t) = -\frac{\partial(\langle \dot{M}_{\rm BH} \rangle n_{\rm BH}(M_{\rm BH}, t))}{\partial M_{\rm BH}} + S_{\rm in} - S_{\rm out},$$
(21)

where $S_{\rm in}$ and $S_{\rm out}$ are, respectively, the merger rate of smaller mass black holes ending up with mass $M_{\rm BH}$ and the merger rate of black holes with initial mass $M_{\rm BH}$ merging into more massive systems. The merger rate of haloes as a function of redshift, mass ratio of the progenitors, and mass of the remnants are taken from from Fakhouri & Ma (2008). We then convert the merger rate of haloes to a merger rate of black holes via the median $M_{\rm BH}$-$M_{\rm halo}$ relation, defined, at all times, by cumulative number matching between the black hole and halo mass functions, which allows us to associate the proper halo merger rate to a given bin of black hole mass. Full details are given in Appendices B and C. We make the limiting case assumption that halo mergers are always followed by black hole mergers after a dynamical friction time. The accuracy of this assumption remains a matter of debate (e.g., Cavaliere & Vittorini 2000; Shen 2009; Shankar 2010, and references therein). The impact of the dynamical friction time delay itself is irrelevant at $z \lesssim 2$ (see Shen 2009).

Figure 13 shows the mass function of the G($z, M_{\rm BH}$) model at $z = 4$, 2, and 0.1 without mergers (dashed lines), including major mergers above a black hole mass-ratio threshold $\xi = 0.5$ (solid lines), and including all mergers above a black hole mass-ratio threshold $\xi = 0.1$ (dotted lines). Mergers have limited effect at $z > 2$, but by $z = 0.1$ they have dramatically boosted the space density of black holes with $M_{\rm BH} > 10^9 M_\odot$, to a level clearly inconsistent with the SWM and Vika et al. (2009) estimates. The discrepancy would be more severe if we did not include mass-dependent ϵ in the G($z, M_{\rm BH}$) model (see Figure 10). We

caution, however, that in this regime the local mass function estimates rely largely on extrapolation of the $M_{\rm BH} - \sigma_*$ or $M_{\rm BH} - M_*$ correlations into a range with limited observational constraints. This is also a mass range where typical galaxy hosts are gas poor, and it is not clear that "dry" galaxy mergers necessarily lead to black hole mergers.

In general, the inclusion of mergers makes it even harder to fit the observed steep decline of black hole abundance at high masses.

5.4   A λ-dependent bolometric correction

The inclusion of mergers puts otherwise acceptable models at risk of overpredicting the high mass end of the local black hole mass function. We now discuss one possible resolution of this tension, a λ-dependent bolometric correction.

Following previous work (e.g., Elvis et al. 1994; Marconi et al. 2004; Shankar et al. 2004; Hopkins et al. 2007), we have so far assumed that the bolometric correction depends only on bolometric luminosity (all the X-ray data in SWM were converted to bolometric luminosities using the L-dependent bolometric correction by Marconi et al. 2004). However, some studies (e.g., Dai et al. 2004; Saez et al. 2008; and references therein) show signs for variations in the spectral energy distributions of AGNs with either redshift or accretion properties. In particular, Vasudevan & Fabian (2007, 2009) suggest that variations in the disc emission in the ultraviolet may be important to build the optical-to-X-ray spectral energy distributions of AGNs. From a sample of 54 AGNs from the Far Ultraviolet Spectroscopic Explorer (FUSE) and X-ray data from the literature, they claim evidence for a large spread in the bolometric corrections, with no simple dependence on luminosity being evident. Their results suggest instead a more well-defined relationship be-
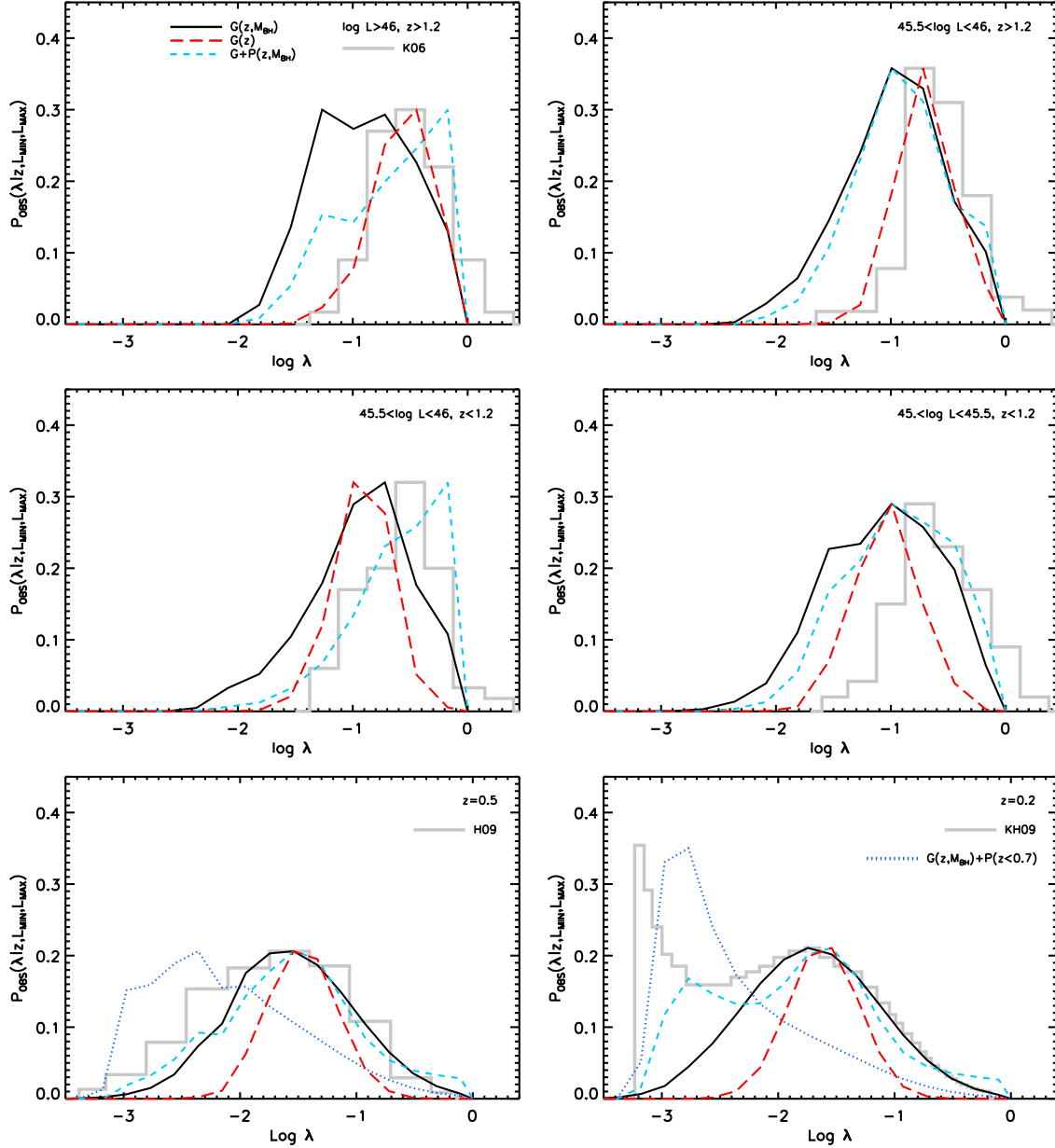
Figure 12. Similar format to Figures 5 and 6. Comparison among the G(z, M_{BH}), G(z) and G+P(z, M_{BH}) predicted Eddington ratio distributions (*solid, red long-dashed*, and *cyan dashed* lines, respectively) compared to the K06 data at $z = 2$ and $z = 1$, respectively (*top* and *middle* panels), and to H09 at $z = 0.5$ (*lower left*) and KH09 in the local Universe (*lower right*). In the lower panels, we also include curves for the steep power-law model introduced in Section 4.4.

tween the bolometric correction and Eddington ratio, with a transitional region at an Eddington ratio of ~ 0.1, below which the X-ray bolometric correction is typically 15-25, and above which it is typically 40-70. As shown in Figure 14, we approximate their results by setting

$$K_{2-10\text{keV}}(\lambda) = \begin{cases} 18 & \text{if } \lambda \leqslant 0.105 \\ 54.85 + 26.78 \log L_X - \\ -11.11 \left(\log L_X\right)^2 & \text{if } 0.105 \leqslant \lambda \leqslant 1 \end{cases}. \tag{22}$$

Our analytic approximation is shown as a solid line in Figure 14, against the binned data by Vasudevan and Fabian (2007; the fit and the data extend to $\lambda > 1$), while the dot-dashed and long-dashed lines are more recent fits from Lusso

et al. (2010) derived from a larger sample. As the latter authors point out, while a trend of bolometric correction with λ might exist, determining its exact slope is still challenging given the large dispersion in the data. In this section we will use Eq. 22 as a reference, noting that the Lusso et al. (2010) fits provide consistent results in the range of interest here.

In our numerical formalism described in Appendix A, it is straightforward to insert a λ-dependent bolometric correction. Given that the relation $L \propto K_{2-10\text{keV}}(\lambda) \times L_X \propto \lambda M_{BH}$, it implies that $L_X \propto [\lambda/K_{2-10\text{keV}}(\lambda)]M_{BH}$. Therefore, having a λ-dependent bolometric correction is equivalent to running the code replacing bolometric luminosities with L_X. We thus solve Eq. 9 for computing the
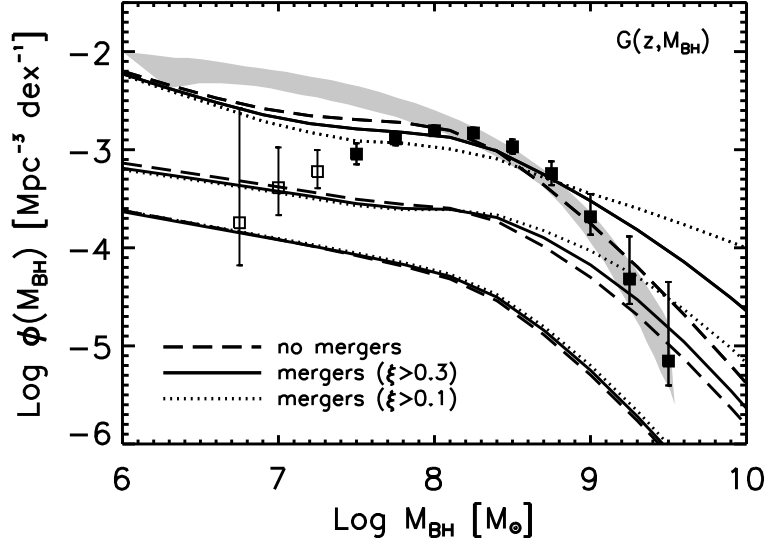
Figure 13. Predicted black hole mass function for the G(z, M_{BH}) model without mergers (*dashed* lines), with only major mergers (*solid* lines), and with minor and major mergers (*dotted* lines). The set of lines, from bottom to top, are the model predictions at $z = 4, 2, 0.1$, respectively. The data are as in Figure 3. The cumulative effect of mergers is minor at $z > 2$ but becomes significant at low redshifts and high masses.
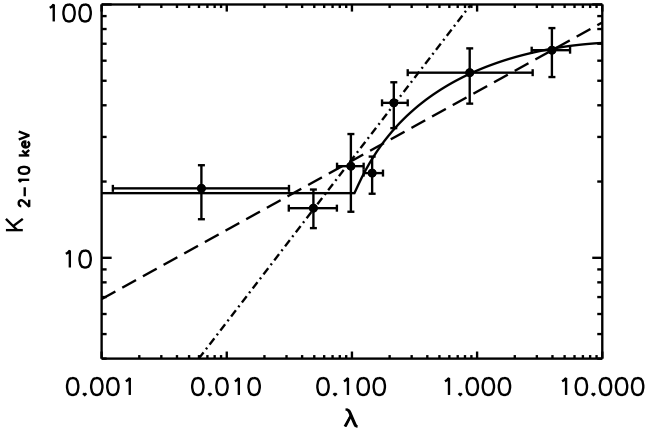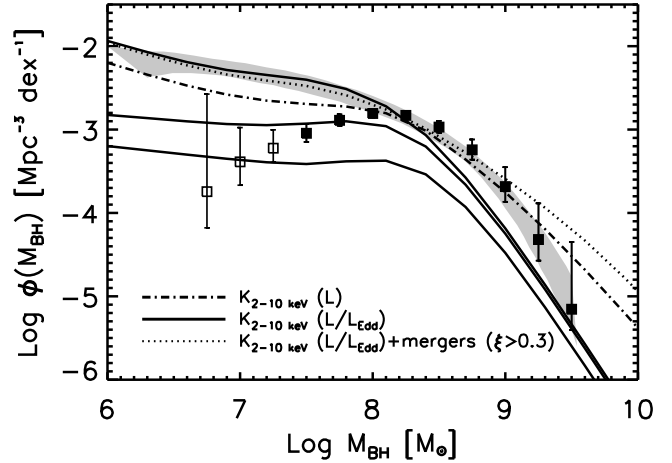

Figure 14. Binned data on the $2 - 10$ keV X-ray bolometric correction as a function of Eddington ratio from Vasudevan & Fabian (2007). The *solid* line is the analytical approximation used in this paper, while the *long-dashed* and *dot-dashed* lines are the results from Lusso et al. (2010).

Figure 15. Influence of a λ-dependent bolometric correction on the predicted black hole mass function. The *dot-dashed* line shows the $z = 0$ mass function of the G(z, M_{BH}) model with our standard bolometric correction. The *solid* lines show the evolving mass function at $z = 2$, 1, and 0 for the same model assuming the λ-dependent bolometric correction of Eq. 22. The dotted line is the λ-dependent G(z, M_{BH}) model inclusive of mergers (with $\xi > 0.3$). Data points and grey band are the same as those in Figs. 3 and 10.

duty cycle by replacing the bolometric luminosity function $\Phi(L, z)$ on the left-hand side with the X-ray luminosity function $\Phi_X(L_X, z)$, and using effective Eddington ratios $\lambda' = \lambda/K_{2-10keV}(\lambda)$.

Most predictions of our models are not sensitive to this change of bolometric correction. In particular, we have checked that after taking into account the λ-dependent conversions between sample flux limits and bolometric luminosities, both duty cycles and Eddington ratio distributions showed similar behaviours to the ones predicted by the G(z, M_{BH}) model with a luminosity-dependent bolometric correction.

Nevertheless, the λ-dependent correction does have a significant effect on the low-z black hole mass function. The solid lines (at $z = 0, 1, 2$, from top to bottom) in

Figure 15 show the G(z, M_{BH}) model with a λ-dependent bolometric correction as in Eq. 22. High-mass black holes have preferentially lower λ in this model, and the lower bolometric luminosity at a given X-ray luminosity reduces the inferred growth rate of these massive black holes. Since G(z, M_{BH}) previously agreed well with the $z = 0$ mass function, it now underpredicts the high mass end.

A λ-dependent bolometric correction would reduce the need for mass-dependent ϵ in our G(z, M_{BH}) and G+P(z, M_{BH}) models (Section 5.1, Fig. 10), which was inferred partly from the high mass end of the local mass func-

tion, though it was also supported by direct empirical evidence for mass-dependent ϵ. Alternatively, a λ-dependent bolometric correction could compensate the impact of mergers on our standard G$(z, M_{\rm BH})$ model (see Fig. 13) to yield improved agreement with local mass function estimates. The dotted line in Figure 15 is the predicted $z = 0$ black hole mass function for the G$(z, M_{\rm BH})$ model including a mass-dependent ϵ, λ-dependent bolometric correction, and black hole mergers with $\xi > 0.3$. Agreement with observational estimates is significantly improved relative to the standard bolometric correction case (uppermost solid line in Fig. 10). Uncertainties in bolometric corrections — their normalization and their dependence on luminosity, λ, or other factors — remain an important source of uncertainty when testing evolutionary models of the black hole population against the local census of black holes.

5.5 Specific Black Hole Accretion Rate

Several authors have noted that the average black hole accretion rate has a redshift dependence morphologically similar to the cosmological SFR (e.g., Marconi et al. 2004; Merloni et al. 2004; Silverman et al. 2008a; Zheng et al. 2009; SWM). Figure 16 adds a new piece of information to the co-evolution of black holes and galaxies, plotting the mean specific accretion rate of black holes of a given mass at a given redshift defined as

$$\frac{\langle \dot{M}(M_{\rm BH}, z)\rangle}{M_{\rm BH}} = \frac{\langle \lambda(M_{\rm BH}, z)\rangle U(M_{\rm BH}, z)}{t_s}. \quad (23)$$

While the mean accretion rate does not depend on the $P(\lambda)$ distribution but only on the assumed radiative efficiency, the mean specific accretion rate depends significantly on the input $P(\lambda)$, so it provides diagnostic power beyond that in the global rates.

In the G(z) model (left panels), the specific mean accretion rate declines with increasing black hole mass at all epochs. Cyan lines in the upper panels show the mean specific star formation rate (SSFR) recently derived by Karim et al. (2011; see also Noeske et al. 2009) at the same redshifts (from their Table 4), with stellar masses simply re-scaled by a factor of 10^{-3} to convert to black hole masses. In this simple comparison with the G(z) model, the mean specific black hole accretion rate decreases with mass and increases with redshift in a remarkably similar way as the mean star formation rate, with a slope $\sim M_{\rm BH}^{-0.4}$. However, when we consider the G$(z, M_{\rm BH})$ model (right panels), which better matches data on black hole duty cycles and λ-distributions, we predict higher specific accretion rates at high masses, reflecting the higher duty cycles in this model. Silverman et al. (2009) also find that in relatively massive high-z galaxies the ratio between average black hole accretion rate and SFR is higher by up to an order of magnitude with respect to the classical 10^{-3}, in fair agreement with the prediction of the G$(z, M_{\rm BH})$ model.

The lower panels of Figure 16 show the mean specific black hole accretion rate as a function of redshift for different bins of black hole mass, as labelled. The grey bands indicate the uncertainties around the measured SSFR as catalogued and derived by González et al. (2010) for galaxies with stellar mass $\sim 5 \times 10^9 - 10^{10} M_\odot$. The latter should be compared with only the specific accretion rate onto black holes with current mass $\sim 10^7 M_\odot$ (solid lines), but for completeness we also show the accretion rate for more massive black holes $M_{\rm BH} = 10^8 M_\odot$ and $M_{\rm BH} = 10^9 M_\odot$ (long-dashed and dotted lines, respectively), as labelled. Overall, consistently with what is found in the upper panels, the models predict an accretion rate that tracks the SSFR, though the G(z) model tends to produce a specific accretion rate that steadily increases even at $z \gtrsim 2$, at variance with the data for the star formation rate. The G$(z, M_{\rm BH})$ model predicts a redshift dependence of the accretion rate morphologically similar to that of galaxies, a fact that might play some role in explaining the still puzzling plateau at $z \gtrsim 2$ of the galactic SSFR(z), which is poorly reproduced by semi-analytic models and might require some extra source of early feedback (e.g., Weinmann et al. 2011).

6 DISCUSSION

Although we have considered a wide variety of models, with different $P(\lambda)$ shapes and different redshift and mass dependences of λ_c and ϵ, every one of these models shows significant (factor of several) disagreement with at least one of the observational tests we have examined. This failure could indicate that our model assumptions are still too restrictive to describe the real black hole population — for example, we generally assume that the shape of $P(\lambda)$ is independent of redshift and black hole mass except for overall shifts in λ_c, and we have considered restricted functional forms for these λ_c trends and for $P(\lambda)$ itself. Alternatively, the problem could lie in one or more of the data sets themselves, since these are frequently derived from noisy or uncertain estimators (e.g., for black hole masses) and from input samples that are subject to selection biases and incompleteness (e.g., for active galaxy fractions). Here we highlight aspects of the data that appear especially difficult to reproduce within our class of models, or where different data sets appear to drive the models in contradictory directions. Recall that all of our models reproduce SWM's estimate of the bolometric luminosity function (summarized in Section 2.2) by construction. SWM discuss remaining uncertainties in this luminosity function and their impact on inferred model parameters.

The first tension within the data is at the low-mass end of the local black hole mass function (see Figure 3), where SWM (and a number of other studies) find a $\Phi(M_{\rm BH})$ rising to low masses but Vika et al. (2009) and some other studies (e.g., Graham et al. 2007) find a falling $\Phi(M_{\rm BH})$. This region of the mass function remains difficult to probe because of uncertainties in bulge-disk decomposition and because the black hole mass correlations for spiral bulges are more uncertain than those for high mass, bulge-dominated galaxies. In our models, it is difficult to produce a turnover like that of Vika et al. (2009), though the G(z) model goes in this direction (Figure 10) because it ascribes much of the low luminosity AGN activity to low-λ accretion by massive black holes, hence reducing the growth of low mass black holes. However, the predicted mass function in this regime depends on the input luminosity function in a range that is largely extrapolated from brighter magnitudes. Therefore if $\Phi(M_{\rm BH})$ really does turn over at low masses, a plausible explanation is that the faint end of the AGN luminosity function is flatter than the one adopted here.
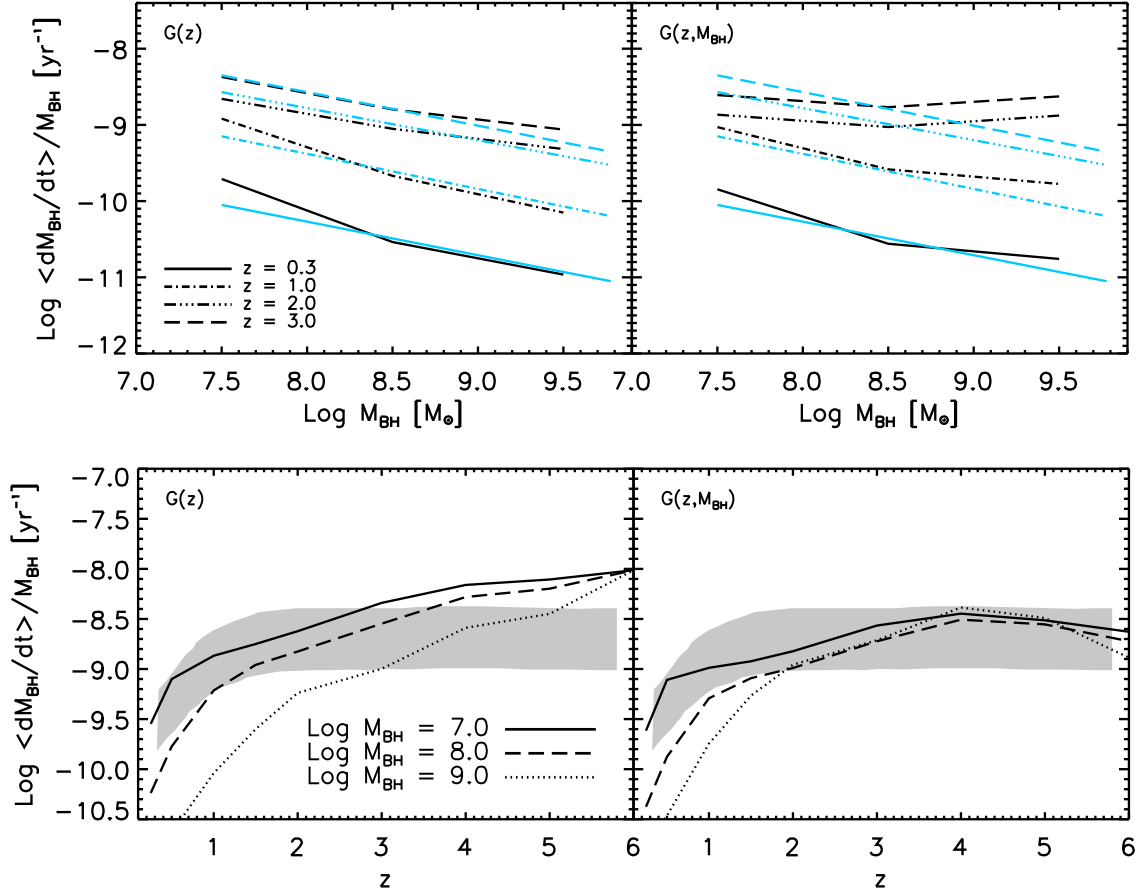
Figure 16. Mean specific black hole accretion rate (Eq. 23) predicted by the G(z) (*left*) and G(z, M_{BH}) (*right*) models as a function of black hole mass (*top*) and of redshift (*bottom*). In the top panels, *cyan* lines are the mean specific star formation rates as calibrated by Karim et al. (2011; their Table 4), with stellar masses simply scaled to black hole masses assuming a proportionality factor of 10^{-3}, as measured in the local Universe. In the bottom panels, the *grey area* is the specific star formation rate with error bars calibrated by González et al. (2010) for galaxies with stellar mass $\sim 5 \times 10^9 - 10^{10} M_\odot$, which can be compared to the predictions for $10^7 M_\odot$ black holes (*solid* curves).

A second tension, with more serious implications for the issues at the core of this paper, is between the narrow Eddington ratio distributions measured by K06 and the broader distribution, peaking at lower λ_c, measured by H09. The two data sets overlap in redshift, though H09 are at the low redshift end of the K06 range. H09, and KH09 at still lower z, favor a $P(\lambda)$ that is broad in shape (like G+P) and evolving to low λ_c at low redshift, but it is difficult to reconcile such a model with the K06 histograms. The luminosity thresholds for the H09 and K06 data sets are very different, roughly $L_{min} = 10^{43}\mathrm{erg\,s}^{-1}$ and $L_{min} = 10^{45}\mathrm{erg\,s}^{-1}$, respectively, so there is no direct contradiction between the measurements. Possibly a model that allows a different *shape* of $P(\lambda)$ for high and low mass black holes, or that allows a power-law that is steeper or further offset from the log-normal peak, could be made consistent with both sets of observations. The two samples might differ for more profound physical reasons, as recently emphasized by Trump et al. (2011), who showed that broad lines might disappear at $\lambda < 0.01$ because of a change in accretion flow structure.

The observed $P(\lambda)$ distributions also include errors in black hole mass estimations, so the intrinsic distributions should in principle be even narrower. Correcting for this ob-

servational broadening would exacerbate the tension with our G(z, M_{BH}) and G+P(z, M_{BH}) models, which already predict broader $P(\lambda)$ distributions than those found by K06.

Another important tension arises between the low duty cycles found for low redshift quasars by Schulze & Wisotzki (2010) and the much higher active galaxy fractions found by Kauffmann et al. (2003), with a gap that is roughly two orders of magnitude. The difference between Type 1 and Type 2 AGN could possibly explain a factor of $10 - 20$ (Greene & Ho 2009), though this factor is already large compared to conventional estimates of obscured-to-unobscured AGN ratios, and other empirical and physical effects might need to be invoked to explain such a strong discrepancy (e.g., Trump et al. 2011). By adopting the Greene & Ho (2009) ratios in our predictions, we find models that are roughly consistent with both Kauffmann et al. (2003) and Schulze & Wisotzki (2010), but even our best cases disagree with one of these data sets by a factor of several in some black hole mass range (see Figure 7). We have converted Kauffmann et al.'s [OIII] luminosities to bolometric luminosities assuming a constant bolometric correction, and scatter or biases in this correction (see, e.g., Capetti 2011) might account for some of the discrepancy with Schulze & Wisotzki (2010). Best et

al. (2005, see their Fig. 2) also find high AGN fractions for SDSS galaxies — $20-40\%$ for $L_{[OIII]} > 10^{5.5} L_{\odot}$ ($\log L \gtrsim 42$) — comparable to those of Goulding et al. (2010).

A fourth tension arises from the trend of higher active fractions for more massive galaxies found by Xue et al. (2010) and Bundy et al. (2010). If $P(\lambda)$ does not evolve, then matching observed AGN luminosity evolution leads to downsizing, i.e., a *decrease* of duty cycle with increasing black hole mass (Figure 3). A $\lambda_c(z)$ that declines towards low redshift can soften this trend, but within our considered range of models, it does not eliminate downsizing entirely. We have been able to produce a trend of rising duty cycle with rising black hole mass by making λ_c decrease towards higher M_{BH}, but the resulting models then tend to be inconsistent with the K06 Eddington ratio distributions, which do not show such a trend (Figure 12). Furthermore, the model trends of $U(M_{BH})$ remain flatter than those found by Xue et al. (2010) and Bundy et al. (2008), and these models still yield falling $U(M_{BH})$ at $z = 0.5$. One caveat is that we are translating the observed galaxy stellar masses to corresponding black hole masses assuming a linear relation with no scatter. If the scatter between black hole mass and galaxy mass were large at these redshifts, then the trend between active fraction and galaxy mass could be partly induced by a higher probability for black holes of fixed mass to be active if they reside in more massive galaxies.

In Section 4.4 we considered a model in which $P(\lambda)$ rises steeply towards low λ (with $P \propto \lambda^{-0.9}$), which helps produce a rising $U(M_{BH})$ trend for a luminosity thresholded sample because more massive black holes can radiate at low λ while remaining above threshold (Aird et al. 2011; Mainieri et al. 2011). We restricted this steep $P(\lambda)$ to $z < 0.7$, since at higher redshifts it leads to duty cycles above unity. With this model (inspired by that of Aird et al. 2011), we are able to obtain a rising $U(M_{BH})$ at $z = 0.5$. However, the prediction for the observed $P(\lambda)$ disagrees with the data of K06, H09, and KH09, a discrepancy also noted by Aird et al. (2011).

A final tension arises at the high end of the black hole mass function, where the models tend to overpredict the data. While models with a mass-independent $P(\lambda)$ are acceptable within the estimated observational uncertainties, adding mass dependence of λ_c to produce a rising $U(M_{BH})$ leads to a substantial overprediction of the abundance of the most massive black holes. We have mitigated this problem in our $G(z, M_{BH})$ model by also increasing the radiative efficiency at high M_{BH} (Figure 10). This solution has some observational support, as discussed in Section 4.3. On the other hand, including mergers as calculated in Section 5.3 worsens the overprediction of $\Phi(M_{BH})$ at high masses (Figure 13).

There are other factors that may ameliorate the discrepancy between models and observational determinations of the abundance of the most massive black holes. A λ-dependent (or simply lower) bolometric correction may resolve this tension, as discussed in Section 5.4. The model shown by the dotted curve in Figure 15, which includes mergers, is acceptable within current uncertainties. The high end of the mass function relies on extrapolation of the M_{BH}-bulge relations into a regime where there are few calibrating galaxies (Schulze & Gebhardt 2011). Another effect that can help fitting the AGN luminosity function with a steeper

decline of the black hole mass function at high masses is an anisotropic emission by AGNs, which would give rise to apparent values of λ (i.e., inferred from the observed flux in our direction under the assumption of isotropy) that are occasionally larger than unity. The majority of the most luminous AGN would then correspond to objects that have their brightest direction of emission pointing to us, rather than to AGN with the highest black hole masses, and the mass accretion rates of these AGN would be lower than their observed luminosities suggest. (Note that in our models we have imposed a cutoff on the $P(\lambda)$ distribution at $\lambda > 1$.)

7   CONCLUSIONS

We have extended the formalism of continuity-equation modeling of the black hole and AGN populations to allow a distribution of Eddington ratios $P(\lambda)$. With this broader class of models we have addressed two new categories of observations, direct estimates of Eddington ratio distributions of active black holes and estimates of duty cycles from active galaxy fractions. Both of these categories have been areas of intense observational investigation over the last five years, and as representative examples we have concentrated on $P(\lambda)$ estimates from Kollmeier et al. (2006; K06) at $z \geqslant 1$, Hickox et al. (2009; H09) at $z \approx 0.5$, and Kauffmann & Heckman (2009; KH09) at $z \approx 1$, and on active galaxy fraction data from Bundy et al. (2008) and Xue et al. (2010) at $z \geqslant 0.5$ and from Goulding et al. (2009), Kauffmann et al. (2003), and Schulze & Wisotzki (2010) at low redshift. We account for the effective luminosity thresholds of these analyses in our model predictions, though the thresholds are not always clearly defined.

As forms for $P(\lambda)$ we consider a Gaussian in $\log \lambda$ (G) and a Gaussian with a power-law extension to low-λ (G+P). If the radiative efficiency ϵ and characteristic Eddington ratio λ_c (where the Gaussian peaks) are held fixed, then changing from a single λ value to either of these distributions has little impact on the evolution of the black hole mass function inferred from continuity-equation modeling. As in the single-λ models of SWM (and similar models by Shankar et al. 2004 and Marconi et al. 2004), we find that models incorporating the observed AGN luminosity function and parameter values $\epsilon \approx 0.07$ and $\lambda_c \approx 0.25$ yield a good match to observational estimates of the black hole mass function in the local Universe. The predicted black hole duty cycle declines rapidly with decreasing redshift at $z < 2$, and at redshifts $z \leqslant 1$ it declines sharply with increasing black hole mass over the range $10^7 M_{\odot} - 10^9 M_{\odot}$ ("downsizing" evolution). An unattractive feature of the G+P model is that it requires a high space density of massive black holes already present at $z = 6$, since only the small fraction of black holes with high λ are luminous enough to contribute to the observed luminosity range at this redshift. This large "seed" population appears physically unrealistic, and the low implied duty cycle for high-luminosity quasars contradicts evidence from their strong observed clustering at $z \approx 4$ (Shen et al. 2007; White et al. 2008; Shankar et al. 2010b). We conclude (in agreement with Cao 2010) that any extended low-λ tail of $P(\lambda)$ must develop at lower redshifts ($z \leqslant 3$) rather than being a redshift-independent feature of black hole fueling processes.

Our models with redshift-independent $P(\lambda)$ predict duty cycles at $z \leqslant 1$ that are far below observational estimates from active galaxy fractions, and they do not match the low-z Eddington ratio distributions estimated by H09 and KH09. Motivated by these discrepancies, we introduce the G(z) model with a redshift-dependent λ_c (Eq. 15), shifting $P(\lambda)$ to lower Eddington ratios at low redshift. This model yields better agreement with the observations, but the low-redshift $P(\lambda)$ remains narrow compared to the H09 and KH09 estimates, and the model still predicts a duty cycle that declines with increasing black hole mass, in contradiction to the Bundy et al. (2008) and Xue et al. (2010) finding of higher AGN fractions in more massive galaxies. We therefore introduce an additional *mass* dependence of λ_c (Eq. 16; $\lambda_c \propto M_{\mathrm{BH}}^{-0.3}$) at each redshift, which, relative to mass-independent models, maps massive black holes to lower luminosity, more numerous AGN. At the same time, we introduce a steady broadening of the Gaussian $P(\lambda)$ towards low redshift (Eq. 17), or, for the G+P model, a steady drop in the minimum Eddington ratio (Eq. 18) that removes the need for an unrealistic seed population at $z = 6$.

The predictions of the resulting models, G(z, M_{BH}) and G+P(z, M_{BH}), are fairly similar. Both models achieve a reasonable match to the H09 and KH09 Eddington ratio distributions, though they underpredict the KH09 distribution at $\lambda \leqslant 10^{-2.5}$. They produce approximate agreement with the low-redshift duty cycle estimates if we adopt the large (factors of $10 - 20$) ratios of Type II to Type I AGN advocated by Greene & Ho (2009), though there are still factor of several discrepancies for some data sets at some M_{BH} values. Both models predict duty cycles that are flat or weakly rising with black hole mass at $z > 1$, thus improving the agreement with Bundy et al. (2008) and Xue et al. (2010), though neither model can reproduce the Xue et al. (2010) trend at $z = 0.5$.

Our models with mass-dependent $P(\lambda|M_{\mathrm{BH}}, z)$ exhibit tension with the K06 Eddington ratio distributions, especially at $z \approx 1$, since the redshift and mass dependence of λ_c drive the predicted $P(\lambda)$ distributions to peak at $\log \lambda \approx -1$ while the observed distributions peak at $\log \lambda \approx -0.6$. Adding a steep ($P \propto \lambda^{-0.9}$) power-law at late times, similar to the model of Aird et al. (2011), can better match the Xue et al. (2010) duty cycle data at $z = 0.5$, but it also spoils the match with the H09 and KH09 Eddington ratio distributions.

Boosting the duty cycle, and thus the growth, of massive black holes tends to overproduce the high-mass end of the local mass function relative to observational estimates. Our standard versions of the G(z, M_{BH}) and G+P(z, M_{BH}) models therefore incorporate a mass-dependent radiative efficiency (Eq. 19), following Cao & Li (2008). The higher efficiency assumed for higher mass black holes reduces their inferred growth, restoring agreement with the local mass function. Alternatively, a λ-dependent bolometric correction (Vasudevan & Fabian 2007) can lower the inferred growth of massive (hence lower λ) black holes in these models, obviating the need for mass-dependent ϵ. However, black hole mergers at the rate suggested by black hole merger statistics also raise the high mass end of the mass function at low redshifts, so in a complete model the mass-dependent ϵ may be be required even with the λ-dependent bolometric correction. Furthermore, Davis & Laor (2011; but see

also Raimundo et al. 2011 and Laor & Davis 2011) have presented direct evidence for mass-dependent ϵ from quasar spectral energy distributions, and such a dependence could also explain the discrepancy between the $\epsilon \gtrsim 0.2$ inferred for luminous, strongly clustered quasars at $z = 4$ (Shankar et al. 2010b) and the average $\epsilon \approx 0.07$ implied by matching the local black hole mass density (SWM and numerous references therein). Each of these arguments for mass-dependent ϵ rests on somewhat shaky ground, but they all point in the same direction. At $z > 1$, the black hole mass functions implied by our models are fairly insensitive to mergers and only moderately sensitive to other model assumptions.

In agreement with previous studies, we find that the growth of the black hole population tracks the overall evolution of the cosmic star formation rate. We also find generally good agreement between the mean *specific* black hole growth rates $\langle \dot{M}_{\mathrm{BH}} \rangle / M_{\mathrm{BH}}$ and Karim et al.'s (2011) estimates of the specific star-formation rates of star-forming galaxies over the full range $0.3 \leqslant z \leqslant 3$, if we simply translate stellar masses to black hole masses with a constant scaling factor of 10^{-3}.

Over the last five years, measurements of AGN clustering have improved dramatically in precision, redshift extent, and luminosity range. These measurements provide valuable constraints on the relation between active black holes and their host dark matter halos, which we have previously explored in the context of single-λ accretion models (Shankar et al. 2010bc). We will extend our clustering studies to include $P(\lambda)$ distributions and mergers in future work.

With $P(\lambda)$ and radiative efficiency allowed to depend on redshift and black hole mass, our models have become rather elaborate despite their simple physical basis. This complexity reflects the growing richness of the observational data, especially the measurements of Eddington ratio distributions and active galaxy fractions over a wide range of redshift, mass, and luminosity, from a variety of data sets. In order of decreasing robustness, our key qualitative conclusions are (a) that the characteristic Eddington ratio λ_c declines at low redshift, (b) that the $P(\lambda)$ distribution broadens at low redshift, (c) that more massive black holes have lower λ_c, and (d) that more massive black holes have higher radiative efficiency.

Despite the flexibility of our models, and despite investigating many variants beyond those discussed in the paper, we have not found a model that reproduces all of the observational constraints we have considered. The remaining discrepancies presumably reflect some combination of inadequate models and systematic errors in the data sets, as discussed in detail in Section 6. On the model side, we have assumed restricted functional forms for the mass and redshift dependence of $P(\lambda)$, and more general behavior or sharper evolutionary transitions may be required to match the data. Observationally, estimates of black hole masses and bolometric luminosities are both subject to systematic uncertainties, and even when these estimates are correct in the mean, scatter can have important effects on inferred trends and distributions. Many of the tensions between the models and the data and among the data sets themselves revolve around the seemingly disparate trends found for optically luminous, broad-line quasars and varieties of low luminosity, Type II AGN. We have followed standard practice in relating these two populations by a simple obscuration factor, but a more nuanced relation between the different categories

of active black holes (e.g., Trump et al. 2011) may be crucial to resolving some of the tensions highlighted here.

Continuity-equation models draw on the inevitable link between luminosity and mass accretion to tie the observable population of AGN to the evolving population of supermassive black holes that power them. They provide a powerful framework for linking empirical studies that probe a variety of observables across a wide span of redshift, luminosity, and black hole mass. As these empirical studies continue to improve in precision, dynamic range, and control of systematic uncertainties, they will refine the models into a tightly constrained history of the cosmic black hole population.

ACKNOWLEDGMENTS

REFERENCES

Adelberger K. L., Steidel C. C., 2005, ApJ, 630, 50
Adelman-McCarthy J. K. et al., 2006, ApJS, 162, 38
Aird J. et al., 2011, arXiv:1107.4368
Aird J. et al., 2010, MNRAS, 401, 2531
Alexander D. M. et al., 2005, ApJ, 632, 736
Alexander D. M. et al., 2008, AJ, 135, 1968
Alexander D. M. et al., 2011, arXiv:1106.1443
Babić A., Miller L., Jarvis M. J., Turner T. J., Alexander D. M., Croom S. M., 2007, A&A, 474, 755
Ballo L. et al., 2007, ApJ, 667, 97
Best P. N., Kauffmann G., Heckman T. M. et al., 2005, MNRAS, 362, 25
Bonoli S., Marulli F., Springel V., White S. D. M., Branchini E., Moscardini L., 2009, MNRAS, 606
Bonoli S., Shankar F., White S. D. M., Springel V., Wyithe J. S. B., 2010, MNRAS, 404, 399
Borys C., Smail I., Chapman S. C., Blain A. W., Alexander D. M., Ivison R. J., 2005, ApJ, 635, 853
Bundy K. et al., 2008, ApJ, 681, 931
Cao X., Li F., 2008, MNRAS, 390, 561
Cao X., 2010, ApJ, 725, 388
Capetti A., 2011, arXiv:1109.6196
Caputi K. I. et al., 2006, A&A, 454, 143
Cavaliere A., Morrison P., Wood K., 1971, ApJ, 170, 223
Cavaliere A., Vittorini V., 2000, ApJ, 543, 599
Chapman S. C., Blain A. W., Smail I., Ivison R. J., 2005, ApJ, 622, 772
Croom S. M. et al., 2005, MNRAS, 356, 415
Croom S. M. et al., 2009, MNRAS, 399, 1755
Dai X., Chartas G., Eracleous M., Garmire G. P., 2004, ApJ, 605, 45

Davis S. W., & Laor A., 2011, ApJ, 728, 98
Di Matteo T., Springel V., Hernquist L., 2005 Nat, 433, 604
Draper A. R. & Ballantyne D. R., 2010, ApJL, 715, L99
Drory N., Salvato M., Gabasch A., Bender R., Hopp U., Feulner G., Pannella M., 2005, ApJ, 619, 131
Eddington A. S., 1922, MNRAS, 83, 32
Elvis M. et al., 1994, ApJS, 95, 1
Erb D. K., Shapley A. E., Pettini M., Steidel C. C., Reddy N. A., Adelberger K. L., 2006, ApJ, 644, 813
Fakhouri O., Ma C.-P., 2008, MNRAS, 386, 577
Fanidakis N., Baugh C. M., Benson A. J., Bower R. G., Cole S., Done C., Frenk C. S., 2011, MNRAS, 410, 53
Ferrarese L., Merritt D., 2000, ApJ, 539, L9
Ferrarese L., Ford H., 2005, SSRv, 116, 523
Fine S. et al., 2008, MNRAS, 390, 1413
Fiore F. et al., 2011, arXiv:1109.2888
Fontana A. et al., 2006, A&A, 459, 745
Foucaud S. et al., 2007, MNRAS, 376, 20
Gawiser E. et al., 2007, ApJ, 671, 278
Gebhardt K. et al., 2000, ApJL, 539, 13
Giocoli C., Tormen G., van den Bosch F. C., 2008, MNRAS, 386, 2135
González V., Labbé I., Bouwens R. J., Illingworth G., Franx M., Kriek M., Brammer G. B., 2010, ApJ, 713, 115
Goulding A. D., Alexander D. M., Lehmer B. D., Mullaney J. R., 2010, MNRAS, 662
Graham A. W., Driver S. P., Allen P. D., Liske J., 2007, MNRAS, 378, 198
Granato G. L., Silva L., Lapi A., Shankar F., De Zotti G., Danese L., 2006, MNRAS, 368L, 72
Greene J. E., Ho L. C., 2007, ApJ, 667, 131
Greene J. E., Ho L. C., 2009, ApJ, 704, 1743
Grier C. J., Mathur S., Ghosh H., Ferrarese L., 2011, ApJ, 731, 60
Haiman Z., Hui L., 2001, ApJ, 547, 27
Häring N., Rix H. W., 2004, ApJ, 604, 89
Heckman T. M. et al., 2004, ApJ, 613, 109
Heckman T. M., Ptak A., Hornschemeier A., Kauffmann G., 2005, ApJ, 634, 161
Hickox R. C. et al., 2009, ApJ, 696, 891
Ho L. C., 2004, Multiwavelength AGN Surveys, 153
Hopkins A., Beacom J. F., 2006, ApJ, 651, 142
Hopkins P. F., Hernquist L., Cox T. J., Robertson B., Di Matteo T., Springel V., 2006, ApJ, 639, 700
Hopkins P. F., Richards G. T., Hernquist L., 2007, ApJ, 654, 731
Hopkins P. F., Hernquist L., 2009, ApJ, 698, 1550
Hughes S. A., Blandford R. D., 2003, ApJ, 585, L101
Islam R. R., Taylor J. E., Silk J., 2004, MNRAS, 354, 427
Karim A. et al., 2011, ApJ, 730, 61
Kauffmann G., Haehnelt M., 2000, MNRAS, 311, 576
Kauffmann G. et al., 2003, MNRAS, 346, 1055
Kauffmann G., Heckman T. M., 2009, MNRAS, 397, 135
Kelly B. C., Vestergaard M., Fan X., Hopkins P., Hernquist L., Siemiginowska A., 2010, ApJ, 719, 1315
Kennicutt R. C. et al., 2003, PASP, 115, 928
Kisaka S., Kojima Y., 2010, MNRAS, 405, 1285
Kocsis B., Sesana A., 2011, MNRAS, 411, 1467
Kollmeier J. A. et al., 2006, ApJ, 648, 128 (K06)
Kochanek, C.S., Eisenstein, D. J., Cool, R. J., et al. 2011, ApJS, submitted, arXiv:1110.4371

Kriek M. et al., 2007, ApJ, 669, 776

Kulkarni G., Loeb A., 2011, arXiv:1107.0517

Lamastra A., Matt G., Perola G. C., 2006, A&A, 460, 487

Laor A., Davis S., 2011, arXiv:1110.0653

Lapi A., Shankar F., Mao J., Granato G. L., Silva L., De Zotti G., Danese L., 2006, ApJ, 650, 42

Lauer T. R., Tremaine S., Richstone D., Faber S. M., 2007, ApJ, 670, 249

Lehmer B. D. et al., 2007, ApJ, 657, 681

Lusso E. et al., 2010, A&A, 512, A34

Metcalf R. B., Magliocchetti M., 2006, MNRAS, 365, 101

Magliocchetti M., Silva L., Lapi A., de Zotti G., Granato G. L., Fadda D., Danese L., 2007, MNRAS, 375, 1121

Magorrian J. et al., 1998, AJ, 115, 2285

Mainieri V. et al., 2011, arXiv:1105.5395

Marchesini D. et al., 2007, ApJ, 656, 42

Marchesini D., van Dokkum P. G., Förster Schreiber N. M., Franx M., Labbé I., Wuyts S., 2009, ApJ, 701, 1765

Marconi A., Risaliti G., Gilli R., Hunt L. K., Maiolino R., Salvati M., 2004, MNRAS, 351, 169

Marconi A. et al., 2008, ApJ, 678, 693

Martini P., Weinberg D. H., 2001, ApJ, 547, 12

Marulli F., Bonoli S., Branchini E., Moscardini L., Springel V., 2008, MNRAS, 385, 1846

Matteucci F., 1994, A&A, 288, 57

McLure R. J., Dunlop. J. S., 2004, MNRAS, 352, 1390

McLure R. J., Jarvis M. J., 2004, MNRAS, 353, L45

Merloni A., 2004, MNRAS, 353, 1035

Merloni A., Rudnick G., Di Matteo T., 2004, MNRAS, 354, L37

Merloni A., Heinz S., 2008, MNRAS, 388, 1011

Metcalf R. B., Magliocchetti M., 2006, MNRAS, 365, 101

Montero-Dorta A. D. et al., 2009, MNRAS, 392, 125

Nandra K., Mushotzky R. F., Arnaud K., Steidel C. C., Adelberger K. L., Gardner J. P., Teplitz H. I., Windhorst R. A., 2002, ApJ, 576, 625

Nandra K., Laird E. S., Steidel C. C., 2005, MNRAS,

Netzer H., Trakhtenbrot B., 2007, ApJ, 654, 754

Netzer H., Lira P., Trakhtenbrot B., Shemmer O., Cury I., 2007, ApJ, 671, 1256

Netzer H., 2009, ApJ, 695, 793

Noeske K. G., 2009, Astronomical Society of the Pacific Conference Series, 419, 298

Osmer P. S., 1982, ApJ, 253, 28

Papovich C., Dickinson M., Giavalisco M., Conselice C. J., Ferguson H. C., 2005, ApJ, 631, 101

Pérez-González P. G. et al., 2008, ApJ, 675, 234

Quadri R. et al., 2007, ApJ, 654, 138

Rafiee A., Hall P. B., 2011, ApJS, 194, 42

Raimundo S. I., Fabian A. C., 2009, MNRAS, 396, 1217

Raimundo S. I., Fabian A. C., Vasudevan R. V., Gandhi P., Wu J., 2011, arXiv:1109.6225

Reddy N. A., Erb D. K., Steidel C. C., Shapley A. E., Adelberger K. L., Pettini M., 2005, ApJ, 633, 748

Richards G. T. et al., 2006, ApJS, 166, 470

Ross N. P. et al., 2009, ApJ, 697, 1634

Rovilos E., Georgantopoulos I., 2007, A&A, 475, 115

Saez C. et al., 2008, AJ, 135, 1505

Salpeter E. E., 1964, ApJ, 140, 796

Salucci P., Szuszkiewicz E., Monaco P., Danese L., 1999, MNRAS, 307, 637

Scannapieco E., Oh S. P., 2004, ApJ, 608, 62 Joo S. J., Yi S. K., Silk

Schulze A., Wisotzki L., 2010, A&A, 516, 87

Schulze A., Gebhardt K., 2011, ApJ, 729, 21

Shankar F., Salucci P., Granato G. L., De Zotti G., Danese L., 2004, MNRAS, 354, 1020

Shankar F., Cavaliere A., Cirasuolo M., Maraschi L., 2008a, ApJ, 676, 131

Shankar F., Dai X., Sivakoff G. R., 2008b, ApJ, 687, 859

Shankar F., Weinberg D. H., Miralda-Escudé, J. 2009, ApJ, 690, 20 (SWM)

Shankar F., 2009, New Astronomy Reviews, 53, 57

Shankar F., Marulli F., Bernardi M., Dai X., Hyde J. B., Sheth R. K., 2010a, MNRAS, 403, 117

Shankar F., Crocce M., Miralda-Escudé J., Fosalba P., Weinberg D. H., 2010b, ApJ, 718, 231

Shankar F., Weinberg D. H., Shen Y., 2010c, MNRAS, 406, 1959

Shankar F., Marulli F., Bernardi M., Boylan-Kolchin M., Dai X., Khochfar S., 2010d, MNRAS, 405, 948

Shankar F., Sivakoff G. R., Vestergaard M., Dai X., 2010e, MNRAS, 401, 1869

Shankar F., 2010, IAU Symposium, 267, 248

Shankar F., Marulli F., Bernardi M., Mei S., Meert A., Vikram V., 2011, arXiv:1105.6043

Shen Y. et al., 2007, AJ, 133, 2222

Shen Y., Greene J. E., Strauss M. A., Richards G. T., Schneider D. P., 2008, ApJ, 680, 169

Shen Y., 2009, ApJ, 704, 89

Shen Y. et al., 2009, ApJ, 697, 1656

Shen Y., Kelly B. C., 2010, ApJ, 713, 41

Shen Y., Kelly B. C., 2011, arXiv:1107.4372

Sheth R. K., Tormen G., 1999, MNRAS, 308, 119

Shi Y., Rieke G., Donley J., Cooper M., Willmer C., Kirby E., 2008, ApJ, 688, 794

Silverman J. D. et al., 2008a, ApJ, 679, 118

Silverman J. D. et al., 2008b, ApJ, 675, 1025

Silverman J. D. et al., 2009, ApJ, 696, 396

Small T. A., Blandford R. D., 1992, MNRAS, 259, 725

Sołtan A., 1982, MNRAS, 200, 115

Smith R. E. et al., 2003, MNRAS, 341, 1311

Steed A., Weinberg D. H., 2003, astroph/0311312

Steinhardt C. L., Elvis M., 2010a, MNRAS, 402, 2637

Steinhardt C. L., Elvis M., 2010b, MNRAS, L72

Tamura N., Ohta K., Ueda Y., 2006, MNRAS, 365, 134

Tinker J., Kravtsov A. V., Klypin A., Abazajian K., Warren M., Yepes G., Gottlöber S., Holz D. E., 2008, ApJ, 688, 709

Trakhtenbrot B., Netzer H., Lira P., Shemmer O., 2011, ApJ, 730, 7

Trump J. R. et al., 2011, ApJ, 733, 60

Ueda Y., Akiyama M., Ohta K., Miyaji T., 2003, ApJ, 598, 886

van Dokkum P. G. et al., 2006, ApJ, 638, 59

Vasudevan R. V., Fabian A. C., 2007, MNRAS, 381, 1235

Vasudevan R. V., Fabian A. C., 2009, MNRAS, 392, 1124

Vestergaard M., 2002, ApJ, 571, 733

Vestergaard M., 2004, ApJ, 601, 676

Vika M., Driver S. P., Graham A. W., Liske J., 2009, MNRAS, 400, 1451

Vittorini V., Shankar F., Cavaliere A., 2005, MNRAS, 363, 1376

Volonteri M., Madau P., Quataert E., Rees M. J., 2005, ApJ, 620, 69

Volonteri M., Sikora M., Lasota J. P., 2007, ApJ, 667, 704

Wandel A., Peterson B. M., Malkan M. A., 1999, ApJ, 526, 579

Wang J.-M. et al., 2009, ApJL, 697, L141

Weinmann S. M., Neistein E., Dekel A., 2011, arXiv:1103.3011

White M., Martini P., Cohn J. D., 2008, MNRAS, 390, 1179

Willott C. J. et al., 2010a, AJ, 139, 906

Willott C. J. et al., 2010b, arXiv:1006.1342

Wyithe J. S. B., Loeb A., 2003, ApJ, 595, 614

Wyithe J. S. B., Loeb A., 2005, ApJ, 621, 95

Xue Y. Q. et al., 2010, ApJ, 720, 368

Yoo J., Miralda-Escudé J., 2004, ApJL, 614, L25

Yoo J., Miralda-Escudé J., Weinberg D. H., Zheng Z., Morgan C. W., 2007, ApJ, 667, 813

Yu Q., Tremaine S., 2002, MNRAS, 335, 965

Yu Q., Lu Y., 2004, ApJ, 602, 603

Yu Q., Lu Y., 2008, ApJ, 689, 732

Zheng X. Z. et al., 2009, ApJ, 707, 1566

APPENDIX A: SOLVING THE CONTINUITY EQUATION WITH BROAD INPUT EDDINGTON RATIO DISTRIBUTIONS

There is not a unique way to solve Eq. 9. Steed & Weinberg (2003) adopted an input parametrical double power-law duty cycle, and tuned the parameters to predict the AGN luminosity function. More recently, a similar technique has been adopted by Cao (2010), who performed a detailed χ^2 to up-to-date AGN luminosity functions at all redshifts, and then solved the continuity equation having full information on the input duty cycle.

Following these previous works, and in particular Cao (2010), at any redshift z we parameterize the input active mass function $N_{\rm act}(M_{\rm BH}, z)$, i.e., the product of the duty cycle and the black hole mass function, by a double-power law of the type

$$N_{\rm act}(M_{\rm BH}, z) = \frac{N_0}{\left(\frac{M_{\rm BH}}{M_{\rm BH}^*}\right)^\alpha + \left(\frac{M_{\rm BH}}{M_{\rm BH}^*}\right)^\beta}. \quad (A1)$$

At all redshifts, we then determine the parameters N_0, α, β, and $M_{\rm BH}^*$ by first computing the convolution with the input Eddington ratio distribution $P(\lambda|M_{\rm BH}, z)$ and then finding the best-fit to the AGN luminosity function

$$\Phi(L, z) = \int d\log\lambda P(\lambda|M_{\rm BH}, z)N_{\rm act}(M_{\rm BH}, z). \quad (A2)$$

Having $N_{\rm act}(M_{\rm BH}, z)$ at all redshifts we then compute the average accretion rate from Eq. 6 and then compute the black hole mass function from the continuity equation in Eq. 1. The duty cycle at all redshifts and black hole masses is then simply computed from the ratio of $N_{\rm act}(M_{\rm BH}, z)$ and the total black hole mass function. The method described above, which we take as a reference throughout the paper, allows one to describe the accretion histories of black holes for any continuous input Eddington ratio distribution. However, it also relies on assuming an a priori shape for the active mass function of black holes.

We have developed another method to solve for the duty cycle in Eq. 9 that does not rely on any a priori shape for the active mass function. We first assume that the active black holes of mass within $M_{\rm BH}$ at a given redshift z with duty cycle $U(M_{\rm BH}, z)$ accrete following a predefined *discrete* Eddington ratio distribution $P_j(M_{\rm BH}, z)$. We take N values of the Eddington ratio $\lambda = \lambda_j$, with $j = 1, .., N$, and set the relative probability for a black hole to accrete at λ_j equal to $P_j(M_{\rm BH}, z)$. The fraction of active black holes accreting at $\lambda = \lambda_j$ at redshift z is then given by $P_j(M_{\rm BH}, z)U(M_{\rm BH}, z)$, and the distribution P_j must be such to satisfy the condition

$$\sum_j P_j(M_{\rm BH}, z)U(M_{\rm BH}, z) = U(M_{\rm BH}, z) \quad (A3)$$

so that the total fraction of active black holes of mass $M_{\rm BH}$ is given by $U(M_{\rm BH}, z)$. We then solve equation (9) numerically by computing the duty cycle at each point $M_{\rm BH}$ in the grid as

$$U(M_{\rm BH}, z) = (P_{j_{MAX}}\Phi_{\rm BH}(M_{\rm BH}, z))^{-1} [\Phi(L, z)|_{L\propto\lambda_{j_{MAX}}M_{\rm BH}} - \quad (A4)$$
$$- \sum_{j\neq j_{MAX}} P_j\Phi_{\rm BH}(M'_{\rm BH}, z)|_{L\propto\lambda_j M'_{\rm BH}; M'_{\rm BH}>M_{\rm BH}}].$$

A black hole of mass $M_{\rm BH}$ can radiate at the maximum luminosity $L \propto \lambda_{j_{MAX}}M_{\rm BH}$ set by the maximum assumed Eddington ratio $\lambda_{j_{MAX}}$. More massive black holes with mass $M'_{\rm BH} > M_{\rm BH}$ can in principle radiate with similar luminosity L but at lower Eddington ratios $\lambda_j < \lambda_{j_{MAX}}$, according to the relation $L \propto \lambda_j M'_{\rm BH}$. Therefore Eq. A4 computes the duty cycle at a given bin around $M_{\rm BH}$ subtracting from the luminosity function computed at the bin $L \propto \lambda_{j_{MAX}}M_{\rm BH}$, the contributions of more massive black holes with $M'_{\rm BH} > M_{\rm BH}$ shining within the same bin around L with lower Eddington ratios.

Note that Eq. A4 is *implicit*, as in order to compute $U(M_{\rm BH}, z)$ it requires knowledge of the duty cycle at higher masses $U(M'_{\rm BH} > M_{\rm BH}, z)$. However, the more luminous sources in the AGN luminosity function with luminosity L_{MAX} can only be produced by the more massive black holes in the grid with mass $M_{\rm BH,MAX}$ accreting at the maximum Eddington ratio $\lambda_{j_{MAX}}$. Therefore we can set

$$U(M_{\rm BH,MAX}, z) = \frac{\Phi(L, z)}{\Phi_{\rm BH}(M_{\rm BH,MAX}, z)}|_{L\propto\lambda_{j_{MAX}}M_{\rm BH,MAX}}, \quad (A5)$$

and then iteratively solve Eq. A5 for lower and lower mass black holes. We have checked that our results are not dependent on the exact choices for the maximum black hole mass in the grid $M_{\rm BH,MAX}$ or the maximum luminosity L_{MAX}, as long as they are sufficiently large (e.g., $\log M_{\rm BH,MAX} > 9.5 - 10$ and $\log L_{MAX} > 48$). For all our models we set to $\lambda_{j_{MAX}} = 1$.

We have checked that the discrete method described above yields consistent results with the continuous method when the same input $P(\lambda|M_{\rm BH}, z)$ distribution is adopted. However, we do not use the discrete method as a reference for several reasons. Being discrete, it generates oscillations in the predicted black hole mass function and duty cycle, absent from the continuous model. Moreover, due to its discrete nature, the former technique sometimes yields discontinuities at late times, especially when a complicated, mass-dependent, mapping between luminosity and halo mass is assumed. Other methods to solve Eq. 1 in the presence of

broad Eddington ratio distributions have been discussed by, e.g., Cao & Li (2008), although those techniques, based on converting luminosity-based $P(\lambda)$ to mass-based ones, work well mainly for Gaussian distributions.

In Section 5.4 we discuss models characterized by a λ-dependent bolometric correction. For this class of models the solution to the continuity equation is still straightforward even in the presence of broad $P(\lambda|M_{\rm BH}, z)$ distributions. The same exact procedure detailed above can be extended to λ-dependent bolometric corrections by making use of the equality $L_{\rm bol} = L_{2-10\,\rm keV} K(\lambda) = \lambda L_{\rm Edd}$ and simply assuming a new scale of "effective" $\lambda' = \lambda/K(\lambda)$ that map X-ray luminosities $L_{2-10\,\rm keV}$ to Eddington luminosities, and using the X-ray luminosity function into Eq. A2 instead of the full bolometric luminosity function.

APPENDIX B: THE MEAN RELATION BETWEEN BLACK HOLE AND HOST HALO MASS

Our models predict, by construction, the duty cycle and black hole mass function at all times during the evolution. It is therefore possible to infer the mean relation between black hole mass and halo mass via the cumulative relation[5] (e.g., Haiman & Hui 2001; Martini & Weinberg 2001; Wyithe & Loeb 2005)

$$\int_{\log \bar{M}}^{\infty} d\log M \, \Phi_H(M, z) d\log M =$$
$$\int_{\log \bar{M}_{\rm BH}}^{\infty} d\log M_{\rm BH} \Phi_{\rm BH}(M_{\rm BH}, z) \quad (B1)$$

with both $\Phi_{\rm BH}$ and Φ_H in units of comoving $\rm Mpc^{-3} \, dex^{-1}$ for $H_0 = 70 \, \rm km\, s^{-1} \, Mpc^{-1}$.

The halo mass function Φ_H is "corrected" to include subhaloes as

$$\Phi_H(M, z) = \Phi_{\rm ST}(M, z) + \int n_{\rm SH}(M, M') \Phi_{\rm ST}(M', z) d\log M',$$
$$(B2)$$

where $\Phi_{\rm ST}(M, z)$ is the Sheth & Tormen (1999)[6] halo mass function and $n_{\rm SH}(M, M')$ is the mass function from Giocoli, Tormen & van den Bosch (2008) which provides the number of subhaloes with *unstripped* mass within M and $M + dM$ contained by haloes of mass M' and $M' + dM'$. Eq. B2 significantly steepens the halo mass function below $M \sim 10^{12} \, \rm h^{-1} \, M_\odot$, as it increases the number of lower mass haloes more, thus somewhat altering the mean correlation between haloes and black holes in this mass regime.

[5] In this work we do not consider any scatter in the median black hole-halo relation. In future work we will probe the most suitable black hole-halo relation against AGN clustering, scatter, subhalo accretion histories. Changing the $M_{\rm BH} - M$ relation would alter the impact of mergers relative to that discussed in Section 5.3, but we expect such changes to be small.

[6] More recent and detailed analysis of the halo mass functions have been performed (e.g., Tinker et al. 2008); however, we here still use the Sheth & Tormen recipe to make contact with previous works and note that the exact choice of halo mass function does not alter our conclusions.

APPENDIX C: COMPUTING BLACK HOLE MERGERS

In the presence of mergers two additional terms should be added on the right hand side of Eq. 1

$$S_{\rm in} = \frac{1}{4} \int_{\xi_{\rm min}}^{1} d\xi \left(\frac{P_{\rm merg,z}}{\Delta t}(\xi, M) n_h \left[M \left(M'_{\rm BH}, z \right), z \right] \frac{dM}{dM_{\rm BH}} \right) \quad (C1)$$
$$+ d\xi \left(\frac{P_{\rm merg,z}}{\Delta t}(\xi, M) n_h \left[M \left(M''_{\rm BH}, z \right), z \right] \frac{dM}{dM_{\rm BH}} \right)$$

is the merger rate of incoming smaller mass black holes with mass $M'_{\rm BH} = M_{\rm BH} \xi/(1+\xi)$ and $M''_{\rm BH} = M_{\rm BH}/(1+\xi)$ that merge into a black hole of final mass $M_{\rm BH}$, and

$$S_{\rm out} = \frac{1}{2} \int_{\xi_{\rm min}}^{1} d\xi \left(\frac{P_{\rm merg,z}}{\Delta t}(\xi, M) n_h \left[M \left(M'_{\rm BH}, z \right), z \right] \frac{dM}{dM_{\rm BH}} \right) \quad (C2)$$
$$+ d\xi \left(\frac{P_{\rm merg,z}}{\Delta t}(\xi, M) n_h \left[M \left(M''_{\rm BH}, z \right), z \right] \frac{dM}{dM_{\rm BH}} \right)$$

is the merger rate of black holes with initial mass $M_{\rm BH}$ that merge into more massive black holes of mass $M'_{\rm BH} = M_{\rm BH}(1+\xi)/\xi$ and $M''_{\rm BH} = M_{\rm BH}(1+\xi)$. In both Eqs. C1 and C2 we set $\xi_{\rm min} = 0.1$ or $\xi_{\rm min} = 0.3$, and add the factor of $1/2$ to avoid double counting; an additional factor of $1/2$ is present in $S_{\rm in}$ to take into account that two black holes merge into one.

The probabilities of halo mergers per unit time as a function of mass ratio, redshift, and remnant mass are taken from Fakhouri & Ma (2008). Following Shen (2009), we then insert a delay between host dark halo and host galaxy merger rate determined by the dynamical friction time of typical haloes of that mass. The probability of black hole mergers per unit time is then simply given by the "delayed" halo merger rate, i.e.,

$$\frac{P_{\rm merg,z'>z}}{\Delta t}(\xi, M) n_h[M(M_{\rm BH}, z), z] = B_h[M, \xi(z), z], \quad (C3)$$

where z' is the actual epoch of the merger of the progenitor haloes (see Shen 2009 for details). By simply knowing, at each timestep, the mapping between infalling halo mass and its central black hole (given by Eq. [B1]), we can then compute the expected average rate for any black hole merger event.

APPENDIX D: A COMPREHENSIVE COLLECTION OF ACTIVE GALAXIES AT DIFFERENT MASSES AND REDSHIFTS

In this Appendix we present an overview of a detailed literature search aimed at extracting an approximate estimate of the duty cycle of active galaxies at redshifts $z \gtrsim 1$ above some given luminosity.

At $z \sim 2$ several estimates of the number density of certain type of galaxies, along with their AGN fraction, have been measured. Caputi et al. (2006) estimated the cumulative number density of K-selected galaxies at high redshifts from the GOODS-Chandra Deep Fields to be $\lesssim 2 \times 10^{-4} \, \rm Mpc^{-3}$. They also found that the majority of the most massive galaxies in their sample, with stellar masses $> 2.5 \times 10^{11} \, M_\odot$, are ultraluminous infrared galaxies, out of which at least 15% show AGN signatures from their X-ray luminosities. They claim the AGN fraction to

decrease by about a factor of two moving to lower masses and lower infrared luminosities, although this may be partly due to selection effects (Caputi et al. 2006).

In order to extract an absolute value of the AGN fraction from the AGN percentage revealed in the Caputi et al. (2006) sample, we need to correct for the fact that the density of galaxies in their sample may be below the actual total number of galaxies of the same mass at the same redshift. Drory et al. (2005) derived the total galaxy stellar mass function at $2 < z < 2.5$ from I and K selected galaxies in the FORS Deep and GOODS Fields, respectively (see also Fontana et al. 2006). More recently, near-IR estimates come from Pérez-González et al. (2008) and Marchesini et al. (2009). Given the large clustering of high redshift massive galaxies (e.g., Foucaud et al. 2007; Magliocchetti et al. 2007; Quadri et al. 2007) field-to-field variations may significantly affect these results (e.g., Marchesini et al. 2007), but the nice agreement with the estimate by van Dokkum et al. (2006) derived from a large area is also reassuring.

We thus find that the K-selected galaxy number density derived by Caputi et al. (2006) amounts to about 60% of the cumulative number density of galaxies in the stellar mass function with mass above $10^{11}\,M_\odot$. We therefore take a mean of $0.15 \times 0.6 \sim 0.1$ as representative of the AGN fraction in galaxies with at $z \sim 2$ of this mass.

Erb et al. (2006) find that only 5 out of 114 Lyman galaxies host AGNs, consistent with previous claims from similar samples by, e.g., Nandra et al. (2002, 2005), Gawiser et al. (2007). Adelberger & Steidel (2005) estimated an AGN duty cycle of about $\sim 15\%$ (although with large error bars) by combining clustering measurements and space densities of AGNs within their large sample of star forming galaxies at $1.8 \lesssim z \lesssim 3.5$. Kriek et al. (2007) instead found from a sample of 20 K-selected galaxies, that the fraction of AGNs inferred from several emission line diagnostics, was $\sim 20\%$ up to 40% for the more massive galaxies, and rapidly dropping at lower masses. The Kriek et al. results are at variance with the AGN fraction estimated in UV-selected galaxies by Erb et al. (2006) but in reasonable agreement with Caputi et al. (2006). However, Kriek et al. (2007) proved that their estimates are actually consistent with those from UV sample. By binning the Erb et al. sample in stellar mass they found in fact that the AGN fraction in galaxies with stellar mass of $10^{11}\,M_\odot$ is about 16% rising to $\sim 40\%$ at higher masses. Similar results were also claimed by Reddy et al. (2005), shown by a filled circle in the same Figure, who estimated that $\sim 25\%$ of their K_s-selected galaxies in the deep *Chandra* fields are active. Note that the Kriek et al. and Erb et al. results are made somewhat uncertain by the fact that we do not have a proper estimate of the comoving abundance of galaxies in their samples. Papovich et al. (2005) also estimated an AGN fraction of 25% among a sample of distant red galaxies, which reduces to an overall 20% if distant red galaxies comprise about 70% of the overall population of massive high redshift galaxies (van Dokkum et al. 2006; Marchesini et al. 2007).

The majority ($\gtrsim 75\%$) of the Submillimeter galaxies observed with deep SCUBA surveys at 850μ and ultradeep X-ray observations from the 2Msec Chandra Deep Field North, have been observed to host a central AGN (Alexander et al. 2005). The mean BH mass has been calibrated to be $\sim 10^8\,M_\odot$ and the mean Eddington ratio distribution peaked around $0.2 < \lambda < 1$ (Borys et al. 2005; Alexander et al. 2008). However, assuming the comoving density of SCUBA galaxies to be less than 1/4 the cumulative number density of K-selected massive galaxies (e.g., Chapman et al. 2005), we get an average AGN fraction of $\sim 17\%$, comparable to the result by Caputi et al. (2006).

At lower redshifts estimates of the AGN fraction in large samples of galaxies have been recently estimated by Bundy et al. (2008), from DEEP2 and AEGIS surveys. In their sample AGNs have been detected in the 2-10 keV hard band of Chandra and therefore they are representative of the overall AGN population (except for highly obscured, Compton thick AGNs). We find the Bundy et al. (2008) stellar mass function to overall in good agreement with other studies, within a factor of ~ 2. The ratio between the active and inactive stellar mass functions estimated by Bundy et al. (2008), yields a duty cycle increasing with black hole mass. The AGN fraction is $\sim 10\%$ raising to $\sim 50\%$ at $z \sim 1.1$, and from 0.01 to 0.1 at $z \sim 0.5$. This result is in good agreement with the estimates by Lehmer et al. (2007) who find that about 5% of the early-type galaxies in the Extended Chandra Deep Field-South contain AGNs in the local universe, increasing as $(1 + z)^3$ at higher redshifts (i.e., about 17% at $z \sim 0.5$). A closer inspection by Silverman et al. (2008b) on an X-ray selected sample at redshifts $0.63 \lesssim z \lesssim 0.76$, has confirmed an AGN fraction of $(15\pm 5)\%$, decreasing to $\sim 2 - 6\%$ for lower luminosity galaxies. Similarly, Shi et al. (2008) find a lower limit of 2% for X-ray selected AGNs at $z \sim 0.5$ in low mass galaxies increasing to $\sim 10\%$ in the more massive systems, in good agreement with what inferred by Bundy et al. (2008). The Bundy et al. (2008) average estimates also agree well with the Montero-Dorta et al. (2009) results on the AGN fraction of galaxies residing in different environments at $z \sim 1$ from AEGIS and DEEP2.